Heterogeneity in surface sensing produces a division of labor in *Pseudomonas aeruginosa* populations

Authors: Catherine R. Armbruster[1], Calvin K. Lee[2,3,4], Jessica Parker-Gilham[1], Jaime de Anda[2,3,4], Aiguo Xia[5], Boo Shan Tseng[8], Lucas R. Hoffman[1,9], Fan Jin[5,6], Caroline S. Harwood[1], Gerard C. L. Wong[2,3,4], Matthew R. Parsek[1]

Affiliations: [1]Deptartment of Microbiology, University of Washington, Seattle, WA, USA; [2]Department of Bioengineering, University of California Los Angeles, CA, USA; [3]Department of Chemistry and Biochemistry, University of California Los Angeles, CA, USA; [4]California NanoSystems Institute, University of California Los Angeles, CA, USA; [5]Hefei National Laboratory for Physical Sciences at the Microscale, University of Science and Technology of China, Hefei 230026, P. R. China; [6]Institute of Synthetic Biology, Shenzhen Institutes of Advanced Technology, Chinese Academy of Sciences, Shenzhen, China, P. R. China; [8]School of Life Sciences, University of Nevada Las Vegas, Las Vegas, Nevada, USA; [9]Department of Pediatrics, University of Washington, Seattle, WA, USA.

Abstract

The second messenger signaling molecule cyclic diguanylate monophosphate (c-di-GMP) drives the transition from planktonic to biofilm growth in many bacterial species. *Pseudomonas aeruginosa* has two surface sensing systems that produce c-di-GMP in response to surface adherence. The current thinking in the field is that once cells attach to a surface, they uniformly respond with elevated c-di-GMP. Here, we describe how the Wsp system generates heterogeneity in surface sensing, resulting in two physiologically distinct subpopulations of cells. One subpopulation has elevated c-di-GMP and produces

biofilm matrix, serving as the founders of initial microcolonies. The other subpopulation has low c-di-GMP and engages in surface motility, allowing for exploration of the surface. We also show that this heterogeneity strongly correlates to surface behavior for descendent cells. Together, our results suggest that after surface attachment, *P. aeruginosa* engages in a division of labor that persists across generations, accelerating early biofilm formation and surface exploration.

Introduction

Pseudomonas aeruginosa is an opportunistic pathogen that engages in a range of surface-associated behaviors and is a model bacterium for studies of surface-associated communities called biofilms. Biofilms are dense aggregates of cells producing extracellular matrix components that hold the community together. The biofilm mode of growth confers cells protection from a variety of environmental stresses including nutrient limitation, desiccation, and shear forces, as well as engulfment by protozoa in the environment or phagocytes in a host (*1*).

The secondary messenger signaling molecule cylic-di-GMP (c-di-GMP) drives the transition from the planktonic to the biofilm mode of growth. In many bacterial species, including *P. aeruginosa*, elevated c-di-GMP results in repression of flagellar motility genes, while promoting expression of genes involved in producing a biofilm matrix(*2*). The *P. aeruginosa* biofilm matrix is composed of a combination of polysaccharides (including Pel and Psl), proteins (including the adhesin CdrA), and extracellular DNA (*3*–*8*). Biofilm matrix production is an energetically costly process that is regulated at multiple levels (*9*). The *cdrA, pel* and *psl* genes are all transcriptionally induced under conditions of high c-di-GMP(*10*).

For many species, the initial step in biofilm formation involves adherence of free swimming planktonic cells to a surface and the initiation of surface sensing. *P. aeruginosa* has at least two distinct surface sensing systems, the Wsp and the Pil-Chp systems, that when activated, lead to biofilm formation. The Wsp system senses an unknown surface-related signal (recently proposed to be membrane perturbation (*11*)) through WspA, a membrane-bound protein homologous to methyl-accepting chemotaxis

proteins (MCPs). Activation of this system stimulates phosphorylation of the diguanylate cyclase WspR, which leads to the formation of aggregates of phosphorylated WspR (WspR-P) in the form of visible subcellular clusters. This aggregation of WspR-P potentiates its activity, increasing c-di-GMP synthesis (*12*). In comparison, the Pil-Chp chemosensory-like system initiates a hierarchical cascade of second messenger signaling in response to a surface (*13*). First, an increase in cellular cAMP levels occurs through activation of the adenylate cyclase CyaB by the chemotaxis-like Pil-Chp complex. This increases expression of genes involved in type IV pilus biogenesis, including PilY1. PilY1 is associated with the type IV pilus and harbors a Von Willebrand motif, which is involved in mechanosensing in eukaryotic systems(*14*). Thus, it has been proposed that this protein may be involved in the mechanosensing of surfaces (*15*). The output of this second signal is through the diguanylate cyclase, SadC, resulting in an increase in cellular c-di-GMP levels. Unlike the Wsp system, which localizes laterally along the cell (*16*), PilY1 is required to be associated with polarly-localized type IV pili in order to stimulate c-di-GMP production (*13*, *14*), suggesting that *P. aeruginosa* deploys both polar and laterally localized systems to promote c-di-GMP synthesis in response to a surface.

Here, we examined the dynamics of c-di-GMP production and bacterial surface motility at the single-cell level during early stages of biofilm formation. We used a plasmid-based, transcriptional reporter of intracellular c-di-GMP to follow the downstream fate of cells producing varying levels of c-di-GMP in response to surface attachment. Within a clonal population of *P. aeruginosa*, we found that levels of c-di-GMP vary among individual cells as they sense a surface, leading to a division of labor

between two energetically costly behaviors associated with early biofilm formation: surface exploration and polysaccharide production.

Results

Cellular c-di-GMP levels rapidly increase upon surface attachment

We initially compared levels of c-di-GMP between *P. aeruginosa* PAO1 cells growing attached to a silicone surface and subjected to constant flow for 4 hours to those grown planktonically for 4 h. As expected, we observed that PAO1 cellular c-di-GMP levels are 4.4-fold higher (± 0.78 SD, N = 3, $p \leq 0.05$) after 4h of growth attached to a surface compared to planktonic growth (Figure 1A). Because direct measurement of c-di-GMP by LC-MS/MS is limited by our ability to generate enough biomass at earlier time points, we used qRT-PCR to monitor *pel* transcript levels as a readout of c-di-GMP. We found that after just 30 min of surface attachment, *pelA* transcript levels had increased almost 10-fold compared to planktonically grown cells (Figure 1 – Supplement 1). This is consistent with previously published literature showing that transcription of the *pel* operon is directly and positively controlled by high cellular levels of c-di-GMP (*17*, *18*).

The P_{cdrA}::*gfp* reporter detects heterogeneity in c-di-GMP during surface sensing

Next, we sought to visualize early c-di-GMP signaling events at the single cell level. To this end we used a plasmid-based, c-di-GMP responsive transcriptional reporter, pP_{cdrA}::gfp_{ASV} (*19*) in two commonly-studied *P. aeruginosa* strains, PAO1 and PA14. Planktonic cells (a condition where the reporter is inactive due to low c-d-GMP levels) were used to inoculate flow cell chambers. We imaged individual cells of each reporter strain hourly for up to 6 hours after surface attachment (Figure 1B and Figure 1 – Supplement 2). As expected, we saw minimal GFP fluorescence at the 0 h time point

(right after surface attachment). However, by 1 h, the reporter was activated in a subset of surface attached cells, as defined by GFP fluorescence greater than twice that of background levels (referred to as reporter "on" subpopulations). Interestingly, between 4 and 6 h post inoculation, we consistently observed that the c-di-GMP reporter was only active in a subset of cells in both strains (Figure 1C). In PA14, the reporter was activated in 10% of the population over 6 h, whereas PAO1 displayed greater reporter activity, with 40-60% of the cells displaying reporter activity through 12 h (Figure 1 – Supplement 2). We confirmed these results using flow cytometry to assess the proportion of attached cells that were fluorescent (Figure 1 – Supplement 3D,E). To be sure that the promoter of *cdrA* is representative of c-di-GMP-regulated gene expression, we replaced P_{cdrA} with the promoter of *siaA*, a gene that is also highly expressed under conditions of elevated c-di-GMP (*10*, *20*). We found that pP_{siaA}::gfp_{ASV} reporter activity resembled that of pP_{cdrA}::gfp_{ASV} in response to a surface (Figure 1 – Supplement 4). Thus, reporter activity is indeed linked to cellular levels of c-di-GMP.

Cyclic di-GMP heterogeneity leads to phenotypic diversification at early stages of biofilm formation

We then wanted to confirm that subpopulations of surface-attached *P. aeruginosa* cells with high and low c-di-GMP reporter activity are truly physiologically distinct from one another. We used TRITC-labeled lectins to stain for two c-di-GMP-induced exopolysaccharides, Psl and Pel (*7*, *21*), the presence of which is indicative of biofilm formation by PAO1 and PA14, respectively. After 4h of attachment to glass, we observed an enrichment of TRITC-conjugated lectin staining in the population of cells with high c-di-GMP reporter activity (Figure 1D and Figure 1 – Supplement 5),

122 demonstrating that the subpopulation of cells with high c-di-GMP is producing more
123 exopolysaccharide than their low c-di-GMP counterparts. As a complementary approach,
124 we separated 4 h surface-grown cells of the reporter strain into reporter "on" and "off"
125 subpopulations using flow-assisted cell sorting (FACS; Figure 1 – Supplement 6). We
126 then applied qRT-PCR to compare Pel and Psl transcript levels in these two populations.
127 Both the *pel* and *psl* operon transcripts were elevated in the reporter "on" subpopulation,
128 relative to the reporter "off" subpopulation (Figure 1E). These data support that, with
129 respect to c-di-GMP signaling, there are at least two distinct subpopulations that arise
130 shortly after surface attachment.

131 The Wsp system is required for surface sensing

132 We next evaluated the relative contributions of the Wsp and Pil-Chp surface
133 sensing systems to surface-induced c-di-GMP production. Strains with mutations in the
134 Pil-Chp chemosensory system were not significantly defective in surface sensing activity.
135 Deletion of the diguanylate cyclase activated through the Pil-Chp system (PAO1 Δ*sadC*)
136 and the gene encoding the putative sensor PilY1 (PAO1 Δ*pilY1*) did not significantly
137 influence reporter activity in response to a surface (Figure 2 – Supplement 1A,B).
138 Whereas both the SadC and PilY1 mutants displayed wild type levels of reporter activity,
139 a mutant lacking the main Type IV pilus filament protein (PAO1 Δ*pilA*) did show a
140 statistically significant defect in reporter activity by 6 h (Figure 2 – Supplement 1B; $p < 0.05$ by T-test). We then mutated the c-di-GMP cyclase gene, *wspR,* to inactivate the
142 Wsp system. In addition, we deleted the gene encoding the methylesterase *wspF*, which
143 locks the system into the active state, regardless of whether cells are surface-associated.
144 We found that PAO1 Δ*wspR* strain exhibited extremely low levels of reporter activity

during the first 6 h after surface attachment (Figure 2A and Figure 2 – Supplement 2). Complementation of PAO1 Δ*wspR* restored wild type levels of activity at all time points (Figure 2 – Supplement 3). As expected, PAO1 Δ*wspF* had a high proportion of reporter active cells (Figure 2A). We repeated these experiments in the lab strain PA14 and saw a similar trend for Wsp and Pil-Chp mutants (Figure 2 – Supplement 4).

Since the Pil-Chp surface sensing apparatus is polarly localized and the Wsp system is localized laterally along the length of the cell body, we examined whether reporter activity correlated with polar versus lateral attachment to the surface. We found that reporter activity was very low in polarly attached cells, while cells attached along the entire length of the cell body displayed a higher proportion of activated cells (Figure 2B). This finding is also consistent with the localization of the Wsp system and its role for early c-di-GMP signaling during surface sensing.

Heterogeneity in c-di-GMP levels among cells correlates with Wsp system activity

The specific activity of purified WspR increases as a function of WspR concentration when the protein is treated with beryllium fluoride to mimic phosphorylation, supporting the idea that formation of subcellular clusters of WspR-P potentiates its diguanylate cyclase activity and leads to elevated c-di-GMP(*12*). Fewer than 1% of wild-type cells grown in broth have a visible WspR-YFP cluster. However, after a short period of growth on an agar surface, WspR-YFP clusters were visible in 30-40% of wild type PAO1 cells, and this is dependent on sensing by the membrane-bound protein WspA, which is laterally distributed in cells (9). To directly link WspR cluster formation with diguanylate cyclase activity at the cellular level and with surface sensing, we constructed a version of the c-di-GMP reporter that expresses mTFP1 instead of GFP

168 (pP_{cdrA}::*mTFP1*) to avoid the issue of spectral overlap with WspR-YFP. We monitored
169 reporter activity in two point mutants of WspR (L170D and E253A) that are driven by an
170 inducible promoter, translationally fused to eYFP and have been previously shown to
171 form large subcellular WspR clusters in a higher percentage of cells than wild-type
172 WspR. The WspR[L170D] protein is highly active for c-di-GMP production, and it forms
173 subcellular clusters in about 75% of agar surface-grown cells. A WspR[E253A] point
174 mutation abolishes diguanylate cyclase activity, but this protein still forms clusters in
175 about 70% of surface-grown cells (*12*). As expected, in the presence of inducer, we
176 observed a large increase in c-di-GMP reporter activity in WspR[L170D], but not
177 WspR[E253A] (Figure 3A, B). We then asked whether the heterogeneity in reporter
178 activity in response to surface attachment correlates with WspR clustering in the
179 WspR[L170D] strain. We found that pP_{cdrA}::*mTFP1* activity was significantly higher in
180 cells with at least one subcellular WspR-eYFP focus in the WspR[L170D] strain
181 compared to cells without a WspR-eYFP focus (Figure 3C; median mTFP1 fluorescence
182 of 345 vs. 320 RFU respectively, Mann-Whitney test, $p < 0.001$). These data indicate that
183 the heterogeneity observed in c-di-GMP signaling after surface attachment is due to the
184 heterogeneity in the activity of the Wsp system, as reflected by subcellular clustering of
185 active WspR-P.

186 We next asked whether the observed heterogeneity in c-di-GMP signaling in
187 response to a surface has a meaningful influence on biofilm formation. This was
188 particularly important since previous published results indicated that a *wspR* mutation
189 had only a small impact on biofilm production (*22*). However, these studies assessed
190 biofilm formation at later stages of biofilm growth that were well beyond initial surface

191 attachment. Therefore, we chose to compare a *wspR* mutant to wild type at earlier
192 biofilm stages. We performed *in vitro* biofilm assays and observed that a PAO1 Δ*wspR*
193 mutant was defective for biofilm formation relative to wild type PAO1 at 2, 4, and 6
194 hours post-attachment (Figure 4A). However, at later stages of development (~24 h), the
195 *wspR* mutant caught up and produced similar amounts of biofilm biomass relative to wild
196 type levels. Complementation of the Δ*wspR* strain *in trans* restored wild type levels of
197 biofilm formation at all time points. These data suggest that the Wsp system rapidly
198 responds to surface contact to generate elevated levels of c-di-GMP, which accelerates
199 biofilm production. Given the importance of c-di-GMP signaling in biofilm production,
200 the fact that the Δ*wspR* strain can ultimately attain wild-stype levels of biofilm biomass
201 suggests that one of the many other known c-di-GMP cyclases present in *P. aeruginosa*
202 may ultimately compensate for c-di-GMP production in the absence of WspR.

203 Cyclic di-GMP heterogeneity leads to diversification in surface exploration at the lineage
204 level

205 We hypothesized that heterogeneity in c-di-GMP signaling dictated by the Wsp complex
206 could impact the surface behavior of the two observed subpopulations. We predicted that
207 the subpopulation of cells with high c-di-GMP after surface attachment would produce
208 biofilm matrix exopolysaccharides and contribute to initial microcolony formation, while
209 the cells with low c-di-GMP would exhibit increased surface motility and detachment,
210 which is known to be inhibited by exopolysaccharide production. To test this hypothesis,
211 we tracked both reporter activity and surface behavior for cells within a single field of
212 view for 40 h. From our single-cell tracking data, we generated family trees across at
213 least four generations of cells, using a previously described technique (*23*). We tracked

the time-averaged P_{cdrA}::*gfp*$_{ASV}$ reporter activity ($I_{c\text{-}di\text{-}GMP}$), surface motility behavior (F_{motile}, defined as the fraction of time that cells are motile), and detachment behavior (tree asymmetry λ where $\lambda = 0$ represents both daughter cells remaining attached to the surface and $\lambda = 1$ represents when one daughter cell detaches or travels outside the field of view).

In *P. aeruginosa*, surface exploration is mainly accomplished by twitching motility, mediated by type IV pili, and does not appear to be influenced by levels of intracellular c-di-GMP when analyzing single cells (*24*). Interestingly, we found that correlations between c-di-GMP and motility during the lifetime of individual cells are weak. However, when analyzing entire lineages in family trees rather than individual cells, we found clear inverse correlations between $I_{c\text{-}di\text{-}GMP}$ and F_{motile} (Figure 4B, $\rho = -0.53$, $p = 0.0012$) and between $I_{c\text{-}di\text{-}GMP}$ and λ (Figure 4C, $\rho = -0.45$, $p = 0.0068$), suggesting that c-di-GMP levels is strongly inversely correlated with surface motility behavior and detachment behavior over multiple generation of cells. To illustrate these correlations, we chose three representative families, with either high, intermediate, or low $I_{c\text{-}di\text{-}GMP}$ and plotted their family trees (Figure 4D) and spatial trajectories (Figure 4E). Families with the highest $I_{c\text{-}di\text{-}GMP}$ had the lowest F_{motile} and λ (Family 1, Figure 4B-E). In these families, daughter cells remained attached following cell division, exhibited continuously elevated c-di-GMP, did not move appreciable distances on the surface, and ultimately produced small microcolonies. In contrast, families of cells with low $I_{c\text{-}di\text{-}GMP}$ had the highest F_{motile} and λ. For these families, daughter cells frequently detached or traveled outside the field of view, had lower c-di-GMP levels, traveled larger distances on the surface, and ultimately did not form microcolonies (Family 3, Figure 4B-E).

One important question is what happens to early biofilm development if we were to effectively remove heterogeneity in c-diGMP output rooted in the WspR surface sensing system. To address this question, we used a strain in which c-di-GMP production could be easily controlled using an optogenetic system. The precise control of c-di-GMP expression in individual cells was made possible by the use of a chimeric protein that fused a diguanylate cyclase domain to a bacteriophytochrome domain. Flow chambers were seeded with the optogenetic strain encoding a heme oxygenase (*bphO*) and light-responsive diguanylate cyclase (*bphS*)(*25*). Initially, cells attached on the glass surface were tracked and continuously stimulated with red-light over ~8 h using adaptive tracking illumination microscopy (ATIM), which allows for precise stimulation of the initial attached cells and their offspring and ensures sustained intracellular c-di-GMP production for a fixed number of surface cell generations (Figure 5 – Supplement 1). Cellular lineages (a cell and all of its offspring) and c-di-GMP expressions were continually monitored for at least 12 h. Families that were not stimulated with light demonstrated a heterogeneous surface response (Figure 5B,D) similar to that of Families 1-3 in Figure 4B-E. Some lineages were dominated by surface explorers, whereas others were seen to commit to microcolony formation. In contrast, in families stimulated with light for more than 1 generation, the resulting c-di-GMP production artificially forced lineages to have low surface motility and commit to microcolony production (Figure 5A,C) similar to that of Family 1 in Figure 4B-E. Families stimulated with light in this manner had higher $I_{c\text{-}di\text{-}GMP}$ and lower λ values than those that were not stimulated (Figure 5 – Supplement 2). We also found that optogenetic control of c-di-GMP results in phenotypes that are consistent with the wild-type behavior presented in Figure 4, with

illuminated cells (high c-di-GMP) displaying the least motility and control (non-illuminated) displaying comparatively greater surface motility (Figure 5 – Supplement 2). Interestingly, families stimulated with light for 1 generation or less are not significantly different from un-illuminated controls (data not shown). Our data show that the generation of c-di-GMP can deterministically lead to the creation of an entire lineage of sessile cells with post-division surface persistence, low motility, and initiation of microcolony formation. Altogether, these results show that c-di-GMP levels, surface motility, and detachment are inversely correlated at the lineage level, and that the time scale for this occurs over multiple generations.

Discussion

Collectively, our data show that heterogeneity in cellular levels of c-di-GMP, generated by the Wsp system in response to surface sensing, leads to two distinct physiological subpopulations. Phenotypic heterogeneity of single cells is a common phenomenon in bacteria that is thought to be beneficial at the population level by allowing a single genotype to survive sudden environmental changes and by promoting a division of labor between costly behaviors that support the growth and survival of the population (*26*). Sources of phenotypic heterogeneity include bistability (*27*) and stochasticity (*28*) of gene expression, unequal partitioning of proteins during cell division due to low abundance (*28*), epigenetic modifications resulting in phase variation (*29*), or through asymmetrical cell division (*30*, *31*). In this study, we show that the Wsp system generates heterogeneity in c-di-GMP signaling, and it is never fully activated in 100% of wild-type, surface-attached cells. Moreover, we show that such heterogeneity results in phenotypic changes for entire family lineages of descendent cells. It is interesting that

283 correlations between c-di-GMP, surface motility, and surface detachment probability are
284 strong when considered for an entire lineage in a bacterial family tree, but weak when
285 considered at the individual cell level. This form of correlation suggests that the
286 enforcement of surface sensing outcomes (ex: the activation of DGCs, attenuation of
287 motility) is slow compared to the cells' division times, and that c-di-GMP signaling is
288 propagated across multiple generations. Additionally, proteins such as DGCs activated
289 by surface sensing may not be passed down to daughter cells equally after division,
290 especially if their number is not large or if they are assymetrically partitioned, which may
291 be one mechanism that leads to the heterogeneity in c-di-GMP levels.

292 If we overwhelm WspR-generated c-di-GMP heterogeneity by using
293 optogentically-induced sustained c-di-GMP production, we find that phenotypic
294 heterogeneity is lost, and that illuminated cells deterministically become sessile and form
295 microcolonies. Interestingly, our optogenetic experiments show that sustained c-di-GMP
296 production for more than one generation is required before commitment to the sessile
297 lifestyle. This observation is consistent with the fact that we see strong correlations
298 between c-di-GMP levels and motility behavior at the lineage level and not at the
299 individual cell level. Moreover, since the WspR surface sensing system generates
300 heterogeneous c-di-GMP levels, this requirement of sustained c-di-GMP production for
301 more than one generation is inherently difficult for wild-type cells to meet, and virtually
302 guarantees the simultaneous existence of motile and sessile subpopulations. This
303 phenotypic heterogeneity, which has been 'hardwired' into the structure of c-di-GMP
304 surface sensing networks, allows for a division of the labor during early biofilm
305 formation, with one subpopulation committing to initiating the protective biofilm

306 lifestyle, while the other subpopulation is free to explore the surface and potentially

307 colonize distant, perhaps more favorable, locations.

308

Materials and Methods

Bacterial strains and growth conditions

The strains, plasmids, and primers used in this study are listed in Table 1. *Escherichia coli* and *P. aeruginosa* strains were routinely grown in Luria–Bertani (LB) medium and on LB agar at 37°C. For the flow cell experiments, *P. aeruginosa* was grown in either LB or FAB minimal medium supplemented with 10mM or 0.6mM glutamate at room temperature (*7*). For flow cytometry experiments, *P. aeruginosa* was grown in either LB medium or in Jensen's defined medium with glucose as the carbon source (*21*). For the tube biofilm and c-di-GMP measurements, *P. aeruginosa* strains were grown in Vogel-Bonner Minimal Medium (VBMM; (*32*)). Antibiotics were supplied where necessary at the following concentrations: for *E. coli*, 100 µg/mL ampicillin, 10 µg/mL gentamicin, and 10 or 60 µg/mL tetracycline; for *P. aeruginosa*, 300 µg/mL carbenicillin, 100 µg/mL gentamicin, and 100 µg/mL tetracycline. P_{cdrA}::gfp_{ASV} reporter and vector control plasmids were selected with 100 µg/mL gentamicin for *P. aeruginosa* strains and 10 µg/mL gentamicin for *E. coli*.

PAO1 Δ*pilY1* was constructed using two-step allelic exchange following conjugation of wild type PAO1 with *E. coli* S17.1 harboring pENTRPEX18Gm::Δ*pilY1* (a gift from Joe Harrison) as previously described (*33*). PAO1 Δ*pilY1* was identified by colony PCR using primers PAO1pilY1-SEQ-F and PAO1pilY1-SEQ-R. PAO1 Δ*dipA* was constructed similarly by conjugation of wild type PAO1 with *E. coli* S17.1 harboring pENTRPEX18Gm::Δ*dipA* (a gift from Joe Harrison). PAO1 Δ*dipA* was identified by colony PCR using primers PAO1dipA-SEQ-F and PAO1dipA-SEQ-R. PA14 Δ*wspR* and

331 Δ*wspF* deletion mutants were confirmed by PCR using primers PA14wspR-SEQ-F and
332 PA14wspR-SEQ-R or PA14wspF-SEQ-F and PA14wspF-SEQ-R, respectively.
333 To create MPAO1 attTn7::P(A1/04/03)::GFPmut, the miniTn7 from pBT270 was
334 integrated into the chromosome of *P. aeruginosa* PAO1 with the helper plasmid pTNS2,
335 as previously described (*34*). pBT270 was created by introducing the constitutive
336 A1/04/03 promoter (*35*) and removing the trc promoter from pBT223 using the
337 QuikChange Lightning Kit (Agilent Technologies) and the oligonucleotides OBT314 and
338 OBT315. pBT223 was constructed via recombineering of pBT200, pUC18-miniTn7T2-
339 Gm-GW, and pBT212 using Multisite Gateway technology (Invitrogen). pBT212 was
340 constructed by cloning the *gfpmut3* from AKN66 using OBT268 and OBT269, and
341 recombining the PCR product with pDONR221 P1-P5r.
342 Construction of optogenetic, c-di-GMP reporter strain in *P. aeruginosa*.
343 Chromosomal insertion of *bphS* was achieved using the mini-CTX system and these
344 strains were marked with different fluorescent proteins by mini-Tn7 site-specific
345 transposition essentially as previously described (*34*, *36*). First, a *bphS* fragment obtained
346 from the plasmid pIND4 was cloned into the vector mini-CTX2 with the *PA1/O4/O3*
347 promoter upstream of the MCS via a two-piece ligation. The constructed plasmid was
348 electroporated into PAO1 and the corresponding recombinant strain was identified by
349 screening on LB agar plates containing 1mM IPTG and 100 µg/mL tetracycline. Then,
350 the strains were electroporated with a pFLP2 plasmid and distinguished on LB agar plates
351 containing 5% (w/v) sucrose for the excision of the resistance marker. The c-di-GMP
352 reporter plasmid and mCherry/EGFP marked *bphS* mutants were constructed as described

353 above. The c-di-GMP reporter plasmid (P_{cdrA}::gfp_{ASV}) was electroporated into the
354 mCherry marked *bphS* mutant to monitor the intracellular c-di-GMP level.

355 Cyclic di-GMP measurement and qRT-PCR of tube biofilms

356 Measurement of c-di-GMP in tube biofilm cells was performed as previously described
357 (*4*). Transcriptional analysis of PelA expression in tube biofilms was performed as
358 described in the "FACS and qRT-PCR of c-di-GMP reporter cells" section.

359 Crystal violet attachment assays

360 Crystal violet assays were performed essentially as previously described to measure
361 biofilm biomass, except using gentle washing after 2-6 hours of static incubation (*8*). To
362 measure biofilm biomass at 24 hours, the crystal violet assay was performed as
363 previously described without gentle washing (*37*).

364 Flow cell time course experiments and confocal microscopy

365 *P. aeruginosa* cells harboring the pP_{cdrA}::gfp_{ASV} reporter plasmid or a promotorless vector
366 control (pMH489) were grown to mid-log in LB with 100 µg/mL gentamicin (Gm100)
367 from LB Gm100 plates or from FAB + 10mM glutamate overnight broth cultures in FAB
368 + 10mM glutamate. Mid-log cells were back diluted into 1% LB or FAB + 0.6mM
369 glutamate and flow chambers were inoculated at a final OD_{600} 0.1 and inverted for 10
370 minutes to allow cells to attach before induction of flow. Clean media was used to wash
371 non-attached cells by flow at 40mL per hour for 20 minutes. Flow was then reduced to a
372 final constant flow rate of 3mL per hour and bacteria were imaged immediately on a
373 Zeiss LSM 510 scanning confocal laser microscope (t=0h). Flow cells were incubated at
374 a constant flow rate at room temperature and imaged hourly for up to 24 hours. For every
375 strain and time point, 5 fields of view and a minimum of 300 cells were captured using

identical microscope settings to image GFP fluorescence across all experiments. Images were analyzed using using Volocity software (Improvision, Coventry, UK). Cells were counted as pP_{cdrA}::*gfp*$_{ASV}$ reporter "on" if their mean GFP fluorescence intensity per pixel was greater than two-fold above the background GFP fluorescence intensity (approximately 340). Data are presented in terms of the percentage of cells with an average GFP fluorescence per pixel twofold more intense compared to the background (pP_{cdrA}::*gfp*$_{ASV}$ reporter "on"). Microscopy images were artificially colored to display GFP fluorescence as green.

Construction of p*PsiaA*::*gfp*

A region 259 bp upstream through 21 bp into the coding sequence of *siaA* was amplified from PAO1 genomic DNA using primers BamH1-Psia-F and SiaA-BamH1-R, then gel purified using a QIAquick gel extraction kit (Qiagen, Hilden, Germany) digested with BamH1, then column purified with a QIAquick PCR purification kit (Qiagen, Hilden, Germany) to remove BamH1. The GFP expression vector pMH487, which contains the *gfp*mut3 gene with an RNase III splice site and lacking a promoter (*38*), was digested with BamH1, treated with Antarctic phosphatase (New England Biolabs, Ipswich, MA), then column purified with a QIAquick PCR purification kit (Qiagen, Hilden, Germany) to remove BamH1. The P*siaA* allele was ligated into digested pMH487, then transformed into *E. coli* DH5α, purified, and sequenced using primer M13F(-21) (Genewiz). The reporter pP_{siaA}::*gfp* was electroporated into *P. aeruginosa* as previously described and maintained under gentamycin selection at 100 μg/mL.

Multi-generation single cell tracking of type IV motility and c-di-GMP reporter activity

Wild type PAO1 harboring the pP_{cdrA}::*gfp*$_{ASV}$ reporter was grown shaking for 20 hours in FAB media with 6mM glutamate. The flow cell inoculum was prepared by diluting the culture to a final OD_{600} of 0.01 in FAB with 0.6mM glutamate. The flow cell inoculum was injected into the flow cell (Department of Systems Biology, Technical University of Denmark) and allowed to incubate for 10 minutes at 30^{o}C prior to flushing with media at 30mL/h for 10 minutes. Experiments were performed under a flow rate of 3mL/hour for a total of 40 hours.

Images were acquired with an Olympus IX81 microscope equipped with a Zero Drift Correction autofocus system, a 100× oil objective with a 2× multipler lens, and an Andor iXon EMCCD camera using Andor IQ software. Bright-field images were recorded every 3 seconds and GFP fluorescence every 15 minutes. Acquisition continued for a total recording time of 40 hours, which resulted in approximately 48000 bright-field images, and 160 fluorescence images.

Images were analyzed in MATLAB to track bacterial family trees, GFP fluorescence, and surface motility essentially as previously described(*23*) with the following modifications. Image analysis, family tracking and manual validation, family tree plotting, and tree asymmetry λ calculations were performed as previously described(*23*) without modification. GFP fluorescence intensities were normalized by calculating the distribution of intensities per cell per frame (extracted by using the binary image as a mask) and then setting the minimum and maximum intensities to the 1st and 99th percentiles of this distribution for each dataset. $I_{c\text{-}di\text{-}GMP}$ (relative normalized c-di-GMP reporter intensity) was calculated by averaging the normalized fluorescence intensities across all members of a family. F_{motile} (fraction of time that cells in a family

421 are motile) was calculated as follows. For each family, every cell trajectory in the family
422 was divided into time intervals. For each time interval, presence or absence of motility
423 was determined using a combination of metrics, including Mean Squared Displacement
424 (MSD) slope, radius of gyration, and visit map. MSD slope quantifies the directionality
425 of movement relative to diffusion. Radius of gyration and visit map are different metrics
426 for quantifying the average distance traveled on the surface. F_{motile} was then calculated by
427 the fraction of these time intervals that have motility. This calculation was modified from
428 the "TFP activity metric" previously described(*23*).

429 Setup of Adaptive Tracking Illumination Microscopy

430 Figure 5 – Supplement 1 shows a schematic of the Adaptive Tracking Illumination
431 Microscopy (ATIM) setup. An inverted fluorescent microscope (Olympus, IX71) was
432 modified to build the ATIM. The modification includes: 1) a commercial DMD-based LED
433 projector (Gimi Z3) was used to replace the original bright-field light source, in which the
434 original lenses in the projector were removed and three-colored (RGB) LEDs were rewired
435 to connect to an external LED driver (ThorLabs) controlled by a single chip microcomputer
436 (Arduino UNO r3); 2) the original bright-field condenser was replaced with an air objective
437 (40× NA = 0.6, Leica); and 3) an additional 850 nm LED light (ThorLabs) was coupled to
438 the illumination optical path using a dichroic mirror (Semrock) for the bright-field
439 illumination. Note that 850 nm LED light is safe light to ensure that the bright-filed
440 illumination does not affect optogenetic manipulation. The inverted fluorescent
441 microscope (Olympus, IX71) equipped with a 100×oil objective and a sCMOS camera
442 (Zyla 4.2 Andor) was used to collect bright-field images with 0.2 frame rate. The bright-
443 field images were further analyzed to track multiple single cells in real time using a high-

444 throughput bacterial tracking algorithm coded by Matlab. The projected contours of
445 selected single cells were sent to the DMD (1280 × 760 pixels) that directly controlled by
446 a commercial desktop through a VGA port. The manipulation lights were generated by the
447 red-color LED (640 nm), and were projected on the single selected cells in real time
448 through the DMD, a multi-band pass filter (446/532/646, Semrock) and the air objective.
449 Our results indicated that feedback illuminations could generate projected patterns to
450 exactly follow the cell movement (Figure 5 – Supplemental 1B) or single cells divisions
451 (Figure 5 – Supplemental 1C) in real time.

452 Manipulation of c-di-GMP expression in single initial-attached cells

453 The bacterial strain PAO1-*bphS*-P*cdrA*-GFP-mCherry was inoculated into a flow cell
454 (Denmark Technical University) and continuously cultured at $30.0 \pm 0.1℃$ by flowing
455 FAB medium (3.0 mL/h). The flow cell was modified by punching a hole with a 5 mm
456 diameter into the channel, and the hole was sealed by a coverslip that allows the
457 manipulation light to pass through. An inverted fluorescent microscope (Olympus, IX71)
458 equipped with a 100× oil objective and a sCMOS camera (Zyla 4.2 Andor) was used to
459 collect bright field or fluorescent images with 0.2 or 1/1800 frame rate respectively. The
460 power density of the manipulation lights was determined by measuring the power at the
461 outlet of the air objective using a power meter (Newport 842-PE). GFP or mCherry was
462 excited using a 480 nm or 565 nm LED lights (ThorLabs) and imaged using single-band
463 emission filters (Semrock): GFP (520/28 nm) or mCherry (631/36 nm). Initial-attached
464 cells were selected to be manipulated using ATIM with the illumination at 0.05 mW/cm^2,
465 which allowed us to compare the results arising from illuminated or un-illuminated

466 mobile cells in one experiment. The c-di-GMP levels in single cells were gauged using
467 the ratio of GFP and mCherry intensities.

468 Lectin staining and flow cytometry

469 Glass culture tubes were inoculated with 1mL of *P. aeruginosa* in LB or Jensen's
470 minimal media at an OD_{600} 0.8 and incubated statically at 37°C for 4 hours. Non-adhered
471 cells were removed by washing three times with 2mL sterile phosphate buffered saline
472 (PBS). Biofilm cells were harvested by vortexing in 1mL PBS with fluorescein-labeled
473 lectins (WFL lectin (100 µg/mL; Vector Laboratories) for Pel, TRITC-labeled HHA (100
474 µg/mL; EY Laboratories) for Psl) and incubated on ice for 5 minutes. Cells were washed
475 3 times to remove non-adhered lectin, resuspended in PBS, and immediately analyzed for
476 GFP and TRITC fluorescence on a BD LSRII flow cytometer (BD Biosciences). Events
477 were gated based on forward and side scatter to remove particles smaller than a single *P.*
478 *aeruginosa* cell and large aggregates.

479 We used PAO1 cells that did not express GFP (wild type PAO1; Figure 1 –
480 Supplement 3A) or constitutively expressed GFP (PAO1 Tn7::P(A1/04/03)::GFPmut;
481 Figure 1 – Supplement 3B) to define a gate for high GFP fluorescence. We validated this
482 gate using a strain in which we expect very high levels of reporter activity (surface grown
483 PAO1 Δ*wspF*Δ*pelA*Δ*pslBCD* harboring pP*cdrA*::*gfp*$_{ASV}$) and saw that 91.6% of cells had
484 high GFP levels (Figure 1 – Supplement 3C), in agreement with our flow cell
485 characterization of this strain (Figure 2A). We determined gating for TRITC using cells
486 that had not been stained with TRITC-conjugated lectin (Figure 1 – Supplement 5A), as
487 well as two strains that overproduced either Psl (Figure 1 – Supplement 5B) or Pel
488 (Figure 1 – Supplement 5C) that were stained with the appropriate TRITC-conjugated

lectin. Our flow cytometry gating procedure accurately gated 99.7% of wild type PAO1 cells (without the P*cdrA* reporter or lectin-staining) as low GFP and low TRITC (Figure 1 – Supplement 5D).

FACS and qRT-PCR of c-di-GMP reporter cells

Static biofilm reporter cells were grown as described above and harvested without lectin staining. Cells were fixed with 6% paraformaldehyde for 20 minutes on ice, then rinsed once with sterile PBS prior to analysis with a FACSAriaII (BD Biosciences, San Jose, CA). Events were gated first to remove debris and large cellular aggregates, and then gated into cells with low and high GFP fluorescence intensity. The low GFP gate was drawn using wild type PAO1 cells without the gfp gene (Figure 1 – Supplement 6A) and the high GFP gate was drawn using both PAO1 Tn7::P(A1/04/03)::GFPmut (Figure 1 – Supplement 6B) and PAO1 Δ*wspF* Δ*pelA* Δ*pslBCD* P_{cdrA}::gfp_{ASV} reporter (Figure 1 – Supplement 6C). As expected, wild type PAO1 pP_{cdrA}::gfp_{ASV} reporter cells that had been harvested after 4 hours of surface attachment to glass in static LB liquid culture displayed subpopulations of high GFP, reporter "on" cells (30.8% of the population) and "off" (57.2%) cells (Figure 1 – Supplement 6D), whereas this same strain grown to mid-log planktonically in LB displayed mostly reporter "off" cells (Figure 1 – Supplement 6E). Cells were sorted at 4°C by flow assisted cell sorting (FACS) to collect 100,000 events into TRIzol LS (Thermo Fisher Scientific, Waltham, MA). RNA was extracted from sorted cells by boiling immediately for 10 minutes and following the manufacturer's instructions for RNA isolation. DNA was digested by treating with RQ1 Dnase I (Promega, Madison, WI) and samples were checked for genomic DNA contamination by PCR to detect *rplU*. Expression of *pelA*, *pslA*, and *ampR* was measured by quantitative

Reverse Transcriptase PCR (qRT-PCR) using the iTaq Universal SYBR Green One-Step kit (Biorad, Hercules, CA) and a CFX96 Touch Real-Time PCR detection system (Bio-Rad, Hercules, CA). The $\Delta\Delta C_q$ was calculated for 3 independent samples of sorted wild type PAO1 P_{cdrA}::*gfp*$_{ASV}$ reporter biofilm cell populations by normalizing PelA and PslA to relative levels of AmpR expression. Data were presented as the average fold change in PelA or PslA expression in the P_{cdrA}::*gfp*$_{ASV}$ sorted "on" population (high GFP) relative to the "off" population (low GFP) for the three biological replicates.

WspR-YFP foci and pP_{cdrA}::*mTFP1* reporter

A version of the p*PcdrA* reporter was constructed in the pBBR1MCS5 plasmid to express mTFP1 instead of GFP, for use with YFP-tagged WspR proteins. The P*cdrA* promoter and an enhanced ribosomal binding site from the gene 10 leader sequence of the T7 phage (g10L) was amplified from pUC18-miniTn7T2-P_{cdrA}-RBSg10L-*gfp*$_{AGA}$ using primers SacI-PcdrA-F and SOE-PcdrA-RBSg10L-R. The primers mTFP1-F and KpnI-mTFP1-R were used to amplify the mTFP1 gene from plasmid pNCS-mTFP1 (Allele Biotech, San Diego, CA). The P_{cdrA}::RBSg10L::*mTFP1* allele was constructed by SOE-PCR using primers SacI-PcdrA-F and Kpn1-mTFP1-R, then pBBR1MCS5 and the SOE PCR product were doubly digested with SacI/KpnI. Digested pBBR1MCS5 was treated with Antarctic phosphatase, then both digests were gel purified and ligated. The ligation was transformed into *E. coli* DH5α, and plasmid from clones growing on LB with 10 μg/mL gentamycin were sequenced with primers M13F and M13F(-21) (GeneWiz). Fluorescence of the pP_{cdrA}::*mTFP1* reporter was measured in Wsp mutants in a fluorimeter (BioTek Synergy H1 Hybrid Reader, BioTek Instruments, Inc., Winooski, VT, USA) and in flow cells to confirm its activity resembled that of pP_{cdrA}::*gfp*$_{ASV}$. The

535 pP*cdrA*::*mTFP1* reporter was electroporated into *P. aeruginosa* strains with the native
536 WspR deleted and harboring an arabinose-inducible copy of WspR-YFP on its
537 chromosome (*12*). Cells were grown on LB agar plates with 100 μg/mL gentamycin and
538 1% arabinose for 10 hours, then transferred to an agar pad for imaging. WspR-YFP foci
539 and mTFP1 fluorescence was imaged using a Nikon Ti-E inverted wide-field
540 fluorescence microscope with a large-format scientific complementary metal-oxide
541 semiconductor camera (sCMOS; NEO, Andor Technology, Belfast, United Kingdom)
542 and controlled by NIS-Elements. WspR-YFP foci were detected as previously described
543 (*12*).
544
545 **Acknowledgements:** We thank Drs. Julie Cass and Paul Wiggins providing the wide-
546 field microscope and cMOS camera to image WspR-eYFP clusters, Drs. Joe J. Harrison
547 and Yasuhiko Irie for the gift of bacterial strains, and Dr. Keiji Murakami for performing
548 c-di-GMP measurements.
549
550

551 Figures

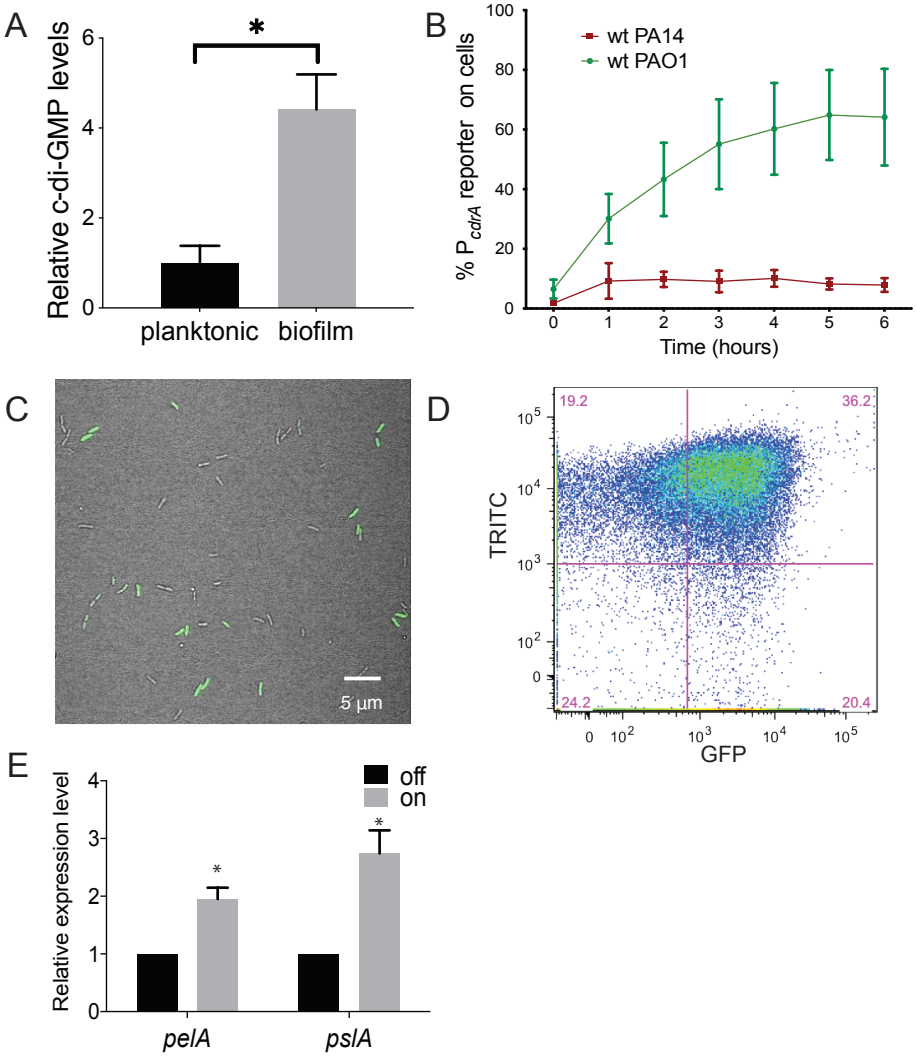

552

553 **Figure 1. Heterogenetity in cellular levels of c-di-GMP during early *P. aeruginosa***

554 **biofilm formation**

555 (A) c-di-GMP levels are elevated rapidly upon association of *P. aeruginosa* PAO1 cells

556 with a surface. Relative levels of intracellular c-di-GMP in wild type PAO1 cells grown

557 either planktonically or after 4 h of attachment to a silicone tube. Values are normalized

558 to the average concentration of c-di-GMP in planktonic cells, in pmol c-di-GMP/mg total

559 protein as determined by LC-MS/MS, and presented as mean and SD. * $p < 0.05$ by T-
560 test, N= 3. Figure 1 – Figure supplement 1 shows the Pel polysaccharide operon is
561 transcriptionally activated almost 10-fold compared to planktonic cells within 30 minutes
562 of surface attachment.
563 (B) Two commonly studied *P. aeruginosa* lab strains, PAO1 and PA14, differentially
564 activate the c-di-GMP reporter during surface sensing. Wild type PAO1 or PA14 cells
565 harboring the c-di-GMP reporter (P_{cdrA}::gfp_{ASV}) were grown to mid-log phase in
566 planktonic culture, then inoculated into a flow cell and supplied with 1% LB medium.
567 Surface attached cells were imaged immediately after inoculation (time 0 h), and hourly
568 for 12 hours. The c-di-GMP reporter is activated in a subset of wild type PAO1 cells
569 within 1 hour of surface attachment and remains activated in approximately 60% of
570 PAO1 cells during the first 6 hours of attachment. In PA14, the c-di-GMP reporter is
571 activated in a smaller proportion of attached cells compared to PAO1. Data points are
572 mean percentage of reporter activated cells from each time point across at least 3
573 biological replicates, with standard deviation. Figure 1 – Supplement 4 shows an
574 additional c-di-GMP responsive transcriptional reporter (using the *siaA* promoter) is also
575 responsive to Wsp-dependent changes in cellular levels of c-di-GMP.
576 (C) Wild type PAO1 cells display heterogeneity in c-di-GMP reporter activity after 6
577 hours of surface attachment. Confocal microscopy image of wild type PAO1 P_{cdrA}::gfp_{ASV}
578 grown in 1% LB after 6 hours of surface attachment during a time course flow cell
579 experiment. Bright field (grey) and GFP (green) channels are merged. Wild type PAO1
580 P_{cdrA}::gfp_{ASV} was grown in 1% LB and imaged by CSLM. Figure 1 – Figure supplement 2
581 shows additional representative timecourse images of PAO1.

582 (D) Psl exopolysaccharide production is enriched in the population of cells with high c-
583 di-GMP. Representative scatterplot of reporter activity versus Psl lectin binding in wild
584 type PAO1 harboring the pP_{cdrA}::gfp_{ASV} reporter grown for four hours in LB before
585 surface attached cells were harvested, stained with the lectin, washed, and counted by
586 flow cytometry.
587 (E) Subpopulations of PAO1 cells with high and low c-di-GMP reporter activity are
588 physiologically distinct. Cells with higher c-di-GMP reporter activity have increased
589 expression of Pel and Psl biosynthetic machinery genes. After 4 hours of attachment to
590 glass, wild type PAO1 cells were separated by flow-assisted cell sorting (FACS) into a
591 population of cells with high (on) and low (off) c-di-GMP reporter activity, then qRT-
592 PCR was performed to quantify expression of Pel and Psl exopolysaccharide biosynthesis
593 genes. Levels of expression of Pel or Psl mRNA were normalized to the off population. *
594 $p < 0.05$ by T-test, N= 3 biological replicates. Figure 1 – Figure supplement 3 shows
595 controls for validating the protocol to monitor pP_{cdrA}::gfp_{ASV} by flow cytometry. Figure 1
596 – Supplement 5 shows by flow cytometry that Psl and Pel polysaccharide production is
597 highest in cells with high pP_{cdrA}::gfp_{ASV} reporter activity.
598 **Figure 1 – Figure supplement 1.** The c-di-GMP-regulated promoter of the Pel
599 polysaccharide operon is transcriptionally activated almost 10-fold compared to
600 planktonic cells within 30 minutes of attachment of PAO1 to a silicone tube. qRT-PCR
601 was performed to detect *pelA* transcript levels in silicone tube biofilm cells compared to
602 planktonic cells (red). Biofilm transcript levels were normalized to planktonic levels at
603 each time point. Colony forming units (CFU) of biofilm attached cells is plotted in
604 yellow at each time point.

Figure 1 – Figure supplement 2. Representative time course images showing the c-di-GMP reporter (P_{cdrA}::gfp_{ASV}) transitioning from inactive upon initial attachment of wild type PAO1 (0 hr) to active in a subpopulation of cells between 1 and 12 hours during a flow cell experiment. A strain harboring the vector control, which encoded gfp_{ASV}, but lacks the P_{cdrA} promoter was imaged alongside each reporter strain (in the appropriate genetic background) to confirm that GFP fluorescence was not due to random expression from the plasmid. Wild type PAO1 P_{cdrA}::gfp_{ASV} was grown in 1% LB and imaged by CSLM. bf = bright field, merge = bright field and GFP channels combined.

Figure 1 – Figure supplement 3. Development of a protocol to monitor pP_{cdrA}::gfp_{ASV} using an LSRII flow cytometer. Brackets indicate gates for "on" (GFP above 1.7×10^2 RFU) or "off" (GFP below 1.7×10^2 RFU) reporter cells and the number above the bracket indicates the percentage of cells that fall within that gate. a) Wild type PAO1 cells were used to determine the background level of fluorescence on the BD Aria III for GFP measurements. The population of cells falls below 10^3 RFU. b) A *P. aeruginosa* strain constitutively expressing stable GFP (PAO1 Tn7::P(A1/04/03)::GFPmut) was used to determine gating for cells with high GFP, with the population ranging from 10^3 to 10^5 RFU. c) Surface grown PAO1 Δ*wspF*Δ*pel*Δ*psl* harboring the pP_{cdrA}::gfp_{ASV} was used to validate the gate for collection of cells with high reporter activity (10^3 to 10^5 RFU; 91.6% of the population). d) Example of gating for reporter "on" cells from wild type PAO1 pP_{cdrA}::gfp_{ASV} cells that had been attached to glass in LB medium for 4 hours. Approximately 56.6% of the population falls into the reporter "on" population. e) Example of gating for "on" cells from wild type PA14 pP_{cdrA}::gfp_{ASV} cells that had been attached to glass in LB medium for 4 hours prior to FACS sorting. Approximately 12.8%

of the population falls into the reporter "on" population. f) Example of gating for "on" cells from wild type PA14 pP_{cdrA}::*gfp*$_{ASV}$ cells that had been attached to glass in Jensen's media (a condition in which Pel is more abundantly produced than in LB) for 4 hours. Approximately 31.9% of the population falls into the reporter "on" population.

Figure 1 – Supplement 4. The *siaA* promoter, regulated by elevated c-di-GMP/FleQ is responsive to Wsp-dependent changes in cellular levels of c-di-GMP. Wild type PAO1 and PAO1 mutants harboring the pP_{siaA}::*gfp* reporter were grown for 20 hours on an LB agar surface with 100 μg/mL gentamycin, resuspended in PBS, and their GFP fluorescence and absorbance at OD_{600} was measured immediately in a spectrophotometer. Asterisk indicates a statistically significant difference in pP_{siaA}::*gfp* reporter activity relative to wild type PAO1 ($p < 0.05$, N = 6, ANOVA with post-hoc Dunnett).

Figure 1 – Supplement 5. Psl and Pel polysaccharide production is highest in cells with high c-di-GMP as measured by the pP_{cdrA}::*gfp*$_{ASV}$ reporter. Brackets indicate gates for polysaccharide-producing, TRITC lectin bound cells (TRITC above 10^3 RFU) or cells without lectin bound (TRITC below 10^3 RFU) on an LSR II flow cytometer and numbers above the brackets indicate the percentage of total cells that fall within the gate. a) Determination of the background level of TRITC autofluorescence in wild type PAO1 that had not been stained with a TRITC-conjugated lectin. b) Determination of the a high level of TRITC-conjugated Psl-specific lectin binding in PAO1 P_{BAD}-psl grown in shaken liquid culture for 4 hours with 1% arabinose before staining with the TRITC-HHA lectin and extensive washing. Approximately 60% of the cells have TRIT-C-HHA lectin bound to their surface. c) Determination of the a high level of TRITC-conjugated Pel-specific lectin binding in PAO1 P_{BAD}-*pel* grown in shaken liquid culture for 4 hours with 1%

arabinose before staining with the TRITC-WFL lectin and extensive washing. Approximately 18.1% of the cells have TRITC-HHA lectin bound to their surface. d) A scatterplot of pP_{cdrA}::gfp_{ASV} reporter activity (GFP) on the x axis and Psl production (as measured by binding of TRITC-HHA lectin to the cell surface) demonstrating the specificity of GFP and TRITC gating in a negative control condition. Wild type PAO1 cells that do not contain the reporter and had not been stained with lectin mostly fall into the lower left quadrant of "off" GFP and no TRITC-lectin binding. The purple numbers in each quadrant represent the percentage of the total population that falls within that quadrant. Quadrants were drawn based on gating of pP_{cdrA}::gfp_{ASV} reporter activity "on" vs. "off" and lectin bound vs. unbound. e) Psl polysaccharide production is enriched in the population of cells with high c-di-GMP. Representative scatterplot of reporter activity versus Psl lectin binding in wild type PAO1 harboring the pP_{cdrA}::gfp_{ASV} reporter grown for four hours in LB before surface attached cells were harvested, lectin stained, washed, and counted by flow cytometry. f) Pel polysaccharide production is enriched in the population of cells with high c-di-GMP. Representative scatterplot of reporter activity versus Pel lectin binding in wild type PA14 harboring the pP_{cdrA}::gfp_{ASV} reporter grown for four hours in Jensen's minimal media plus glucose before surface attached cells were harvested, lectin stained, washed, and counted by flow cytometry.

Figure 1 – Supplement 6. Development of a protocol to sort biofilm cells by pP_{cdrA}::gfp_{ASV} using flow assisted cell sorting (FACS). Brackets indicate gates for "on" (GFP above 1.1 x 10^2 RFU) or "off" (GFP below 10^2 RFU) reporter cells on a BD Aria III flow cytometer and the number above the bracket indicates the percentage of cells that fall within that gate. a) Wild type PAO1 cells were used to determine the background

674 level of fluorescence on the BD Aria III for GFP measurements. The population of cells
675 centers around zero RFU. b) A *P. aeruginosa* strain constitutively expressing stable GFP
676 (PAO1 Tn7::P(A1/04/03)::GFPmut) was used to determine gating for cells with high
677 GFP, with the population centering around 10^3 RFU. c) PAO1 Δ*wspF*Δ*pel*Δ*psl* harboring
678 the pP$_{cdrA}$::*gfp*$_{\mathrm{ASV}}$ was used to draw a gate for collection of cells with high reporter
679 activity (80% of the population). d) Example of gating for reporter "off" and "on" cells
680 from wild type PAO1 pP$_{cdrA}$::*gfp*$_{\mathrm{ASV}}$ cells that had been grown on a surface for 4 hours
681 prior to FACS sorting. Approximately 30% of the population falls into the reporter "on"
682 population. A gap was left between the sorted "off" and "on" populations to increase the
683 stringency of the sorting. e) Example of the "off" and "on" gates drawn on wild type
684 PAO1 pP$_{cdrA}$::*gfp*$_{\mathrm{ASV}}$ cells that were grown planktonically to mid-log, demonstrating that
685 the surface dependent nature of P*cdrA* reporter activity can be detected by flow
686 cytometry.
687
688
689
690

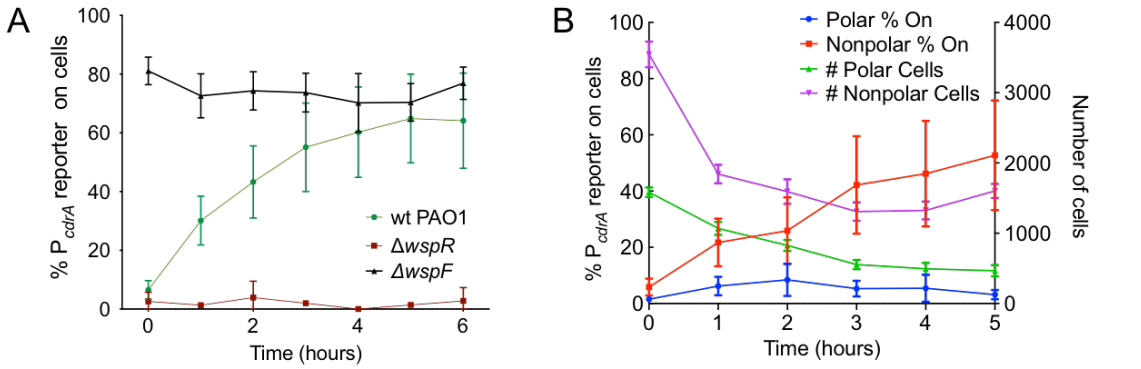

Figure 2. The Wsp system generates heterogeneity in cellular levels of c-di-GMP during early *P. aeruginosa* biofilm formation.

(A) The Wsp system is required for activation of the pP_{cdrA}::*gfp*$_{ASV}$ reporter during surface sensing. Six hour time course plot of the average percentage of surface-attached cells from either wild type PAO1 (green), PAO1 Δ*wspR* (red), or PAO1 Δ*wspF* (black) in which the pP_{cdrA}::*gfp*$_{ASV}$ reporter had turned "on" at each hour. Cells were identified as "on" if their average GFP fluorescence was greater than twice the average background GFP fluorescence of the image. Error bars = standard deviation. N ≥ 3 biological replicates. See Figure 2 – Figure supplement 1 for the same timecourse using mutants in the Pil-Chp surface sensing system. Figure 2 – Figure supplement 2 shows representative images from Figure 2A. Figure 2 – Figure supplement 3 shows that complementing the *wspR* mutant restores wild type levels of reporter activity. Figure 2 – Figure supplement 4 shows that the lab strain PA14 also displays Wsp-dependent c-di-GMP heterogeneity.

(B) Laterally attached cells have higher c-di-GMP levels than polarly attached cells. Five hour time course plot depicting, on the left axis, the percentage of pP_{cdrA}:*gfp*$_{ASV}$ reporter "on" cells that were either polarly (blue) or laterally (red) attached to the surface of a glass coverslip in a flow cell at each hour. The right axis depicts the total number of polar

(green) and laterally attached (purple) cells at each time point. Cells were identified as pP$_{cdrA}$:*gfp*$_{ASV}$ reporter "on" if their average GFP fluorescence was greater than twice the average background GFP fluorescence of the image. Error bars = standard deviation. N = 4 biological replicates.

Figure 2 – Figure supplement 1. Mutants predicted to inactivate the Pil-Chp surface sensing system largely retain pP$_{cdrA}$::*gfp*$_{ASV}$ reporter activity during the first six hours of surface sensing. a) Representative images from wild type PAO1, PAO1 Δ*sadC*, PAO1 Δ*pilY1*, and PAO1 Δ*pilA* after 6 hours of surface attachment. bf = bright field, merge = bright field and GFP channels combined. b) Six hour time course plot of the average percentage of cells from either wild type PAO1 (green), PAO1 Δ*sadC* (red), PAO1 Δ*pilY1* (black), or PAO1 Δ*pilA* (blue) in which the pP$_{cdrA}$::*gfp*$_{ASV}$ reporter had turned "on" at each hour. PAO1 Δ*pilA* is significantly different from wild type PAO1 from 2-6 hours (T-test, $p < 0.05$). Cells were identified as "on" if their average GFP fluorescence was greater than twice the average background GFP fluorescence of the image. Plotted values are the mean of at least 3 biological replicates and error bars are standard deviation.

Figure 2 – Figure supplement 2. The pP$_{cdrA}$::*gfp*$_{ASV}$ reporter is sensitive to Wsp-dependent variation in c-di-GMP during surface sensing. Representative images from wild type PAO1, PAO1 Δ*wspR*, and PAO1 Δ*wspF*Δ*pelC*Δ*pslD* after 6 hours of surface attachment. bf = bright field, merge = bright field and GFP channels combined.

Figure 2 – Figure supplement 3. Complemented diguanylate cyclase mutants display wild type levels of P*cdrA*::*gfp*$_{ASV}$ reporter activity. PAO1 Δ*wspR* and PAO1 Δ*sadC* were complemented at a neutral site on the chromosome under control of their native

promoters. a) Representative images from wild type PAO1, PAO1 Δ*wspR* attCTX::*wspR* (Δ*wspR::wspR*), and PAO1 Δ*sadC* Tn7::*sadC* (PAO1 Δ*sadC::sadC*) after 6 hours of surface attachment. bf = bright field, merge = bright field and GFP channels combined. b) Six hour time course plot of the average percentage of cells from either wild type PAO1 (green), PAO1 Δ*wspR* attCTX::*wspR* (blue), or PAO1 Δ*sadC* Tn7::*sadC* in which the pP_{cdrA}::gfp_{ASV} reporter had turned "on" at each hour. Cells were identified as "on" if their average GFP fluorescence was greater than twice the average background GFP fluorescence of the image. Error bars = standard deviation, n ≥ 3 biological replicates.

Figure 2 – Figure supplement 4. Activity of the pP_{cdrA}::gfp_{ASV} reporter in strain PA14 is dependent on the Wsp system. a) Representative images from wild type PA14, PA14 Δ*wspR*, and PA14 Δ*wspF* after 6 hours of surface attachment. bf = bright field, merge = bright field and GFP channels combined. b) Six hour time course plot of the average percentage of cells from either wild type PA14 (green), PA14 Δ*wspR* (red), or PA14 Δ*wspF* (black) in which the pP_{cdrA}::gfp_{ASV} reporter had turned "on" at each hour. Cells were identified as "on" if their average GFP fluorescence was greater than twice the average background GFP fluorescence of the image. Error bars = standard deviation, n ≥ 3 biological replicates.

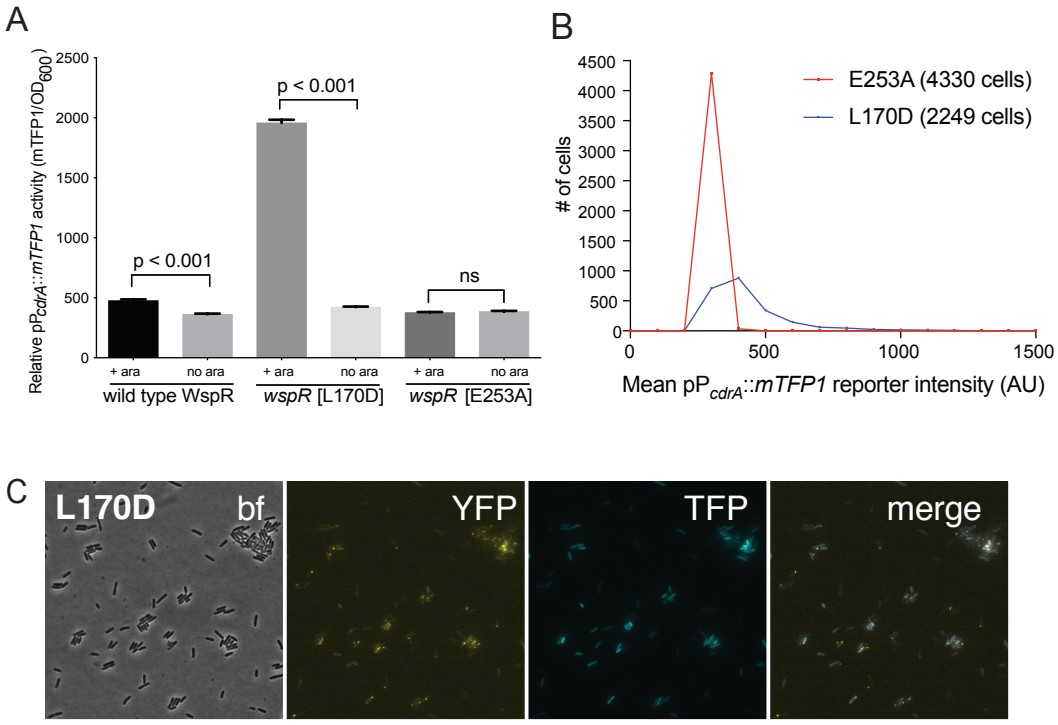

754

755 **Figure 3. Activity of the pP$_{cdrA}$::*mTFP1* reporter is dependent on the ability of**

756 **WspR to produce c-di-GMP.**

757 (A) The pP$_{cdrA}$::*mTFP1* reporter is active in surface grown cells with functional,

758 arabinose-inducible alleles of WspR when arabinose is added to the media. Wild type

759 WspR represents the strain PAO1 Δ*wspR* attCTX::*wspR*-eYFP. *wspR*[L170D] represents

760 the strain PAO1 Δ*wspR* attCTX::*wspR*[L170D]-eYFP, which produces large subcellular

761 clusters of WspR and grows as rugose small colonies on LB with 1% arabinose, a

762 phenotype that is indicative of high intracellular c-di-GMP. *wspR*[E253A] represents the

763 strain PAO1 Δ*wspR* attCTX::*wspR*[L170D]-eYFP cells, which forms large subcellular

764 WspR clusters, but does not produce c-di-GMP via WspR due to the point mutation

765 located in its active site. Cells were grown on LB agar plates with 100 µg/mL gentamicin,

766 and in the presence or absence of 1% arabinose. Cells were resuspended in PBS and

767 mTFP1 fluorescence and OD_{600} were measured. Relative pP_{cdrA}::*mTFP1* reporter activity
768 is the level of mTFP1 fluorescence normalized to OD_{600}. Asterisk indicates statistical
769 significance by Student's t-test ($p < 0.001$) in 6 technical replicates. Error bars = standard
770 deviation.
771 (B) The pP_{cdrA}::*mTFP1* reporter displays heterogeneity in a strain with a functional WspR
772 (*wspR*[L170D]) and is consistently dark in a strain with inactive WspR. Histogram
773 displaying the distribution of average cellular levels of mTFP1 fluorescence from
774 expression of the pP_{cdrA}::*mTFP1* reporter in either the PAO1 Δ*wspR*
775 attCTX::*wspR*[L170D]-eYFP (blue) or PAO1 Δ*wspR* attCTX::*wspR*[L170D]-eYFP (red)
776 backgrounds.
777 (C) Cells with visible subcellulars clusters of WspR[L170D]-eYFP (strain PAO1 Δ*wspR*
778 attCTX::*wspR*[L170D]-eYFP) also have high levels of c-di-GMP reporter activity. bf,
779 bright field; YFP, wspR-YFP foci; mTFP1 = pP_{cdrA}::*mTFP1* activity; and merge, merged
780 YFP and TFP channels. PAO1 Δ*wspR* attCTX::*wspR*[L170D]-eYFP cells harboring the
781 pP_{cdrA}::mTFP1 reporter were grown on LB agar plates with 1% arabinose and 100 µg/mL
782 gentamicin, then spotted onto an agar pad and imaged immediately.
783
784
785

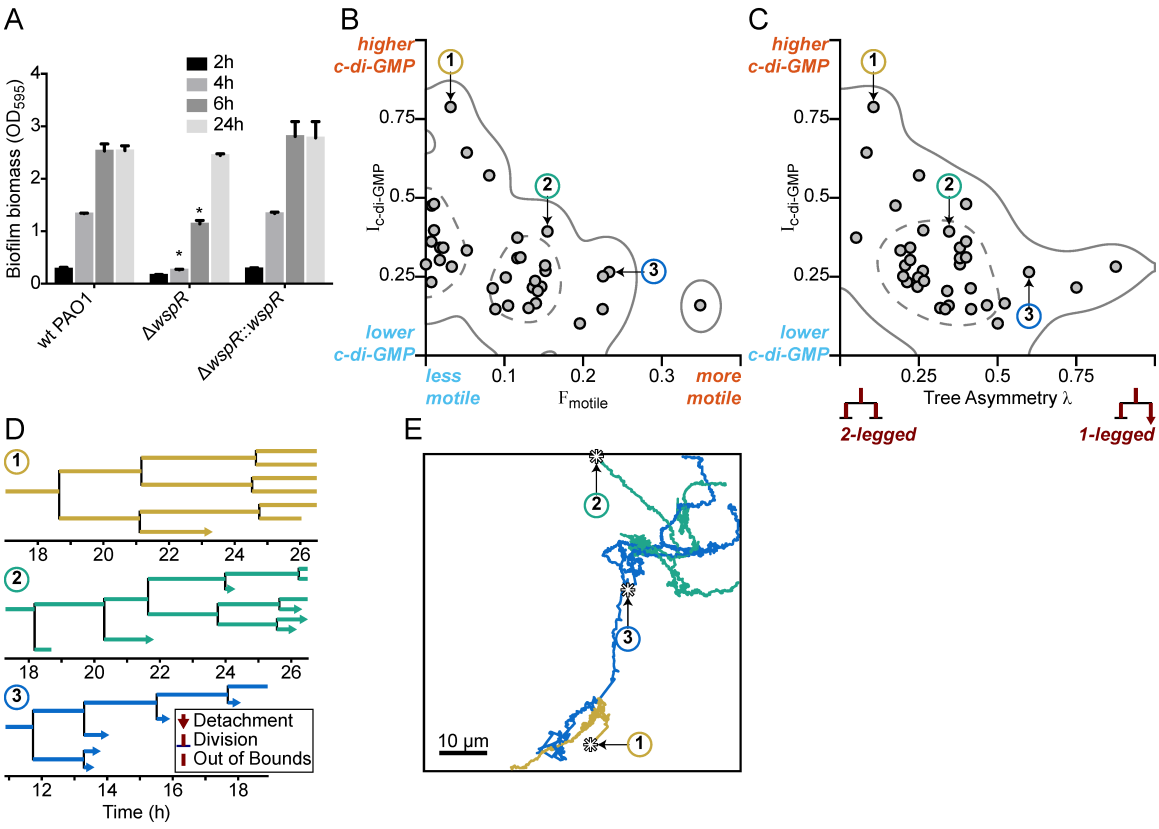

Figure 4. Multigenerational c-di-GMP levels within populations of surface-attached wild type PAO1 cells are inversely correlated with surface motility and detachment.

(A) The Wsp surface sensing system is involved in the early stages of biofilm formation in PAO1. Static biofilm assay performed in wild type PAO1, a single deletion mutant of *wspR*, and the PAO1 Δ*wspR* mutant complemented with w*spR*. Between 4 and 6 hours, PAO1 Δ*wspR* shows a defect in surface attachment and biofilm formation relative to the wild type. However, after 24 hours, PAO1 Δ*wspR* formed equal biofilm biomass compared to wild type. Plotted values are the mean of 6 technical replicates and error is standard deviation. Asterisk indicates a statistically significant change in biomass relative to wild type PAO1 at each time point (Student's t test; $p < 0.05$).

(B) Plot of $I_{c\text{-}di\text{-}GMP}$ vs F_{motile} for individual wild type PAO1 families. $I_{c\text{-}di\text{-}GMP}$ is the relative normalized c-di-GMP reporter intensity averaged across all members of a family.

799 F_{motile} is the fraction of time that cells in a family are motile (specifically surface
800 translational motility). Each circle represents an individual family (N = 35) with at least 4
801 tracked generations. Solid lines represent the 95% probability bounds and dashed lines
802 represent the 50% probability bounds, calculated via kernel density estimation. Spearman
803 correlation: $\rho = -0.53$, $p = 0.0012$.
804 (C) Plot of $I_{c\text{-}di\text{-}GMP}$ vs tree asymmetry λ for individual wild type PAO1 families. Colored
805 numbers indicate the same 3 families from (B) and (D). Tree asymmetry λ quantifies the
806 detachment behavior of family trees as follows. $\lambda = 0$ corresponds to ideal trees with
807 purely "two-legged" division-branching, when both daughter cells remain attached to the
808 surface. $\lambda = 1$ corresponds to ideal trees with purely "one-legged" division-branching
809 when one daughter cell detaches or travels outside the field of view. Points here are the
810 same families as in (B). Solid lines represent the 95% probability bounds and dashed
811 lines represent the 50% probability bounds, calculated via kernel density estimation.
812 Spearman correlation: $\rho = -0.45$, $p = 0.0068$.
813 (D) Family trees of the same 3 representative wild type PAO1 families indicated in (B)
814 and (C). Time 0 h is the start of the dataset recording. Lengths of horizontal lines on the
815 plots are proportional to time spent in each generation. Horizontal lines that end with
816 arrows are detachment events, lines that intersect with a vertical line are division events,
817 and lines that end without a marker are out-of-bound events where we lose track of the
818 bacterium (moving out of the field of view or reaching the end of the recording;
819 represented as moving outside the XYT limits of the dataset boundaries). Vertical lines
820 are arbitrarily spaced to show all the descendants. Colors represent the families in (B) and
821 (C).

822 (E) Spatial trajectories of the 3 representative families. Asterisks (*) represent the initial
823 location of the founder cell. Scale bar 10 μm. The families are color coded as in the
824 previous panels.

825

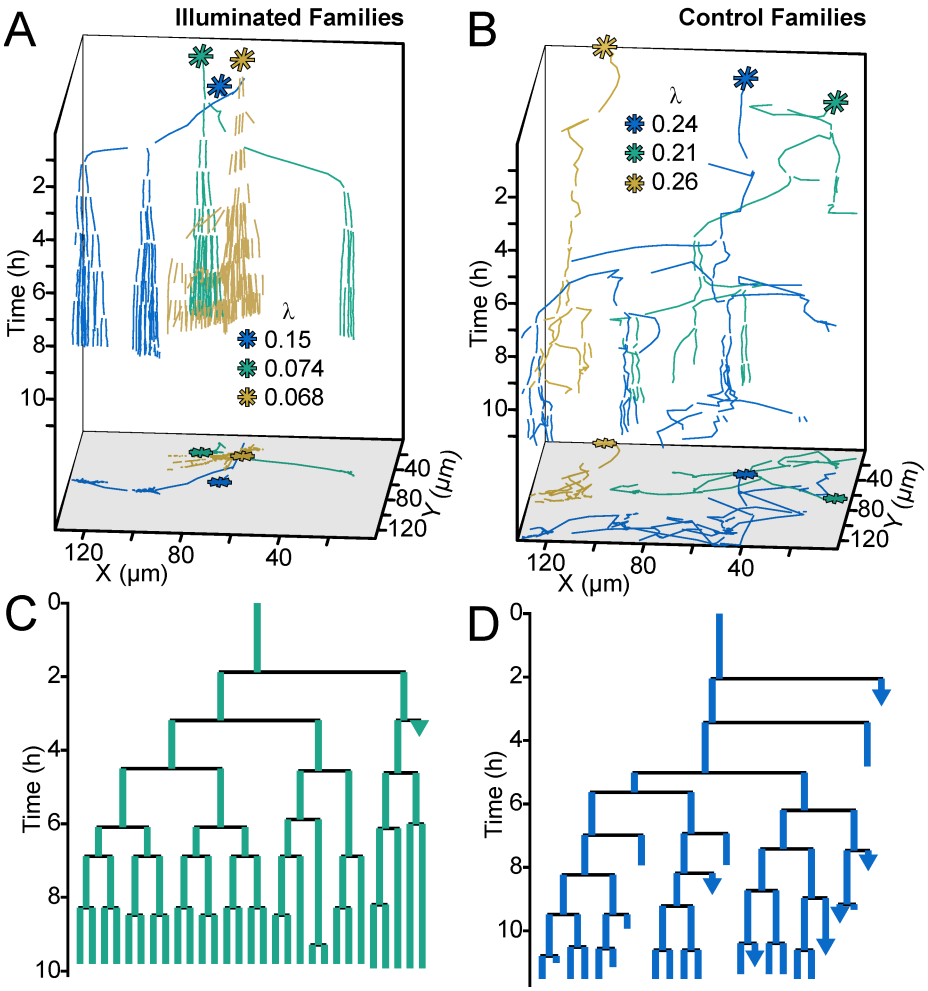

826

827 **Figure 5. Optogenetic control of c-di-GMP production drastically affects family**

828 **architecture and surface motility.**

829 (A,B) Spatiotemporal plot of 3 illuminated families (A) and 3 control families (B). The

830 individual cell tracks in the 3D plot are projected onto the XY plane as spatial

831 trajectories. As in figure 4, λ is a measure of tree asymmetry, with higher values

832 indicating more cells traveling outside the field of view or detaching. In A, the

833 illuminated families tend to be sessile, as expected for cells with high c-di-GMP. In B,

834 control cells are more motile than the illuminated cells in A.

835 (C,D) Family trees of a single corresponding family in (A) and (B), where the color

836 corresponds to the same family. Illuminated cells (C) tend to stay adhered across multiple

837 generations, whereas control cells (D) display more surface motility and detachments.
838 See Movie 1 for a representative video of the optogenetic reporter experiment. Figure 5 –
839 Figure supplement 1 shows a schematic of the ATIM apparatus. Figure 5 – See Figure
840 supplement 2 for the data from Figure 5 overlayed onto Figure 4C, showing that
841 ptogenetic-controlled families follow the trend of family behavior observed in wt PAO1
842 cells.

843 **Figure 5 – Figure supplement 1.** Using Adaptive Tracking Illumination Microscopy
844 (ATIM) to exactly illuminate single *P. aeruginosa* cells on surface. (a) Schematic
845 drawing of the ATI system. A high-throughput bacterial tracking algorithm was
846 employed for analyzing cells' behavior in real time and the information was immediately
847 fed back to an adaptive microscope equipped with a digital micromirror device (DMD).
848 (b) Example depicting one cell of interest being tracked and projected in real time. (c)
849 The feedback illumination can generate projected patterns to exactly follow the daughter
850 cells after the tracked cell divides. Scale bar for all images is 5μm.

851 **Figure 5 – Figure supplement 2.** Optogenetic-controlled families follow the trend of
852 family behavior observed in wt PAO1 cells, with illuminated families resembling the
853 high c-di-GMP matrix producers and control families resembling low c-di-GMP surface
854 explorers. Families plotted in Figure 5 (plus one additional control family) are plotted on
855 top of Figure 4C ($I_{c\text{-}di\text{-}GMP}$ vs λ). Red triangles and blue triangles represent the
856 illuminated and control families, respectively, while the original data from Figure 4C is
857 greyed out. Illuminated families have higher $I_{c\text{-}di\text{-}GMP}$ and lower λ than the control
858 families.

Movie 1. Single cells are precisely illuminated by ATIM via *in situ* analysis and tracking of bacteria. The left panel shows the merged images of gfp_{ASV} and mCherry fluorescence microscopy images over time. The right panel shows the merged images of red LED projected patterns and bright field images corresponding to the left panel. The fluorescence intensity of gfp_{ASV} in the illuminated cells and their offspring (colored red in right panel) is significantly increased after using ATI for 460 mins. In contrast, the gfp_{ASV} fluorescence intensity of the un-illuminated cells remains low and these cells remain motile.

Table 1.

Strains, primers, and plasmids used in this study.

***P. aeruginosa* Strains**		**Reference**
PAO1	wild-type	Holloway, 1979
PA14	wild-type	Rahme, 1995
PAO1Δ*wspF*	markerless, in frame deletion of WspF	Hickman, 2005
PAO1Δ*wspF*Δ*pelA*Δ*pslBCD*	markerless, in frame deletions of WspF, PelA, and PslBCD genes	Rybtke, 2012
PAO1Δ*wspR*	markerless, in frame deletion of WspR	Hickman, 2005
PAO1Δ*pilY1*	markerless, in frame deletion of PilY1	this study
PAO1Δ*sadC*	markerless, in frame deletion of SadC	Irie, 2012
PAO1Δ*pilA*	markerless, in frame deletion of PilA	Shrout, 2006
PAO1Δ*dipA*	markerless, in frame deletion of DipA	this study
PAO1Δ*wspR* attCTX::P*wspA*::*wspR*	PAO1ΔwspR complemented with WspR under control of the Wsp operon promoter and including intergenic region upstream of WspR	Gift from Yasuhiko Irie

PAO1Δ*sadC* attCTX::*sadC*	PAO1ΔsadC complemented with SadC under control of its native promoter	Gift from Yasuhiko Irie
MPAO1 attTn7::P(A1/04/03)::GFPmut	wild type MPAO1 constitutively expressive stable GFP	this sudy
PA14 Δ*wspF*	markerless, in frame deletion of WspF	Gift from Caroline Harwood
PA14 Δ*wspR*	markerless, in frame deletion of WspR	Gift from Caroline Harwood
PAO1Δ*wspR* attCTX::PBAD-wspR-eYFP	markerless, in frame deletion of WspR with arabinose-inducible, C-terminally eYFP-tagged wild type WspR allele	Huangyutitham, 2013
PAO1Δ*wspR* attCTX::PBAD-wspR[L170D]-eYFP	markerless, in frame deletion of WspR with arabinose-inducible, C-terminally eYFP-tagged WspR[L170D] allele	Huangyutitham, 2013
PAO1Δ*wspR* attCTX::PBAD-wspR[E253A]-eYFP	markerless, in frame deletion of WspR with arabinose-inducible, C-terminally eYFP-tagged WspR[E253A] allele	Huangyutitham, 2013
***P. aeruginosa* Reporter Strains**		
PAO1 pMH489		Rybtke, 2012
PAO1 pP*cdrA*::*gfp*ASV		Rybtke, 2012
PAO1 pP*siaA*::*gfp*ASV		this study
PA14 pMH489		this study
PA14 pP*cdrA*::*gfp*ASV		this study
PAO1Δ*wspF* pMH489		this study
PAO1Δ*wspF* pP*cdrA*::*gfp*ASV		this study
PAO1Δ*wspF* pP*siaA*::*gfp*		this study
PAO1Δ*wspF*Δ*pelC*Δ*pslD* pMH489		this study
PAO1Δ*wspF*Δ*pelC*Δ*pslD* pP*cdrA*::*gfp*ASV		this study
PAO1Δ*wspR* pMH489		this study
PAO1Δ*wspR* pP*cdrA*::*gfp*ASV		this study
PAO1Δ*wspR* pP*siaA*::*gfp*		this study
PAO1Δ*pilY1* pMH489		this study
PAO1Δ*pilY1* pP*cdrA*::*gfp*ASV		this study
PAO1Δ*sadC* pMH489		this study
PAO1Δ*sadC* pP*cdrA*::*gfp*ASV		this study
PAO1Δ*pilA* pMH489		this study
PAO1Δ*pilA* pP*cdrA*::*gfp*ASV		this study
PAO1Δ*dipA* pMH489		this study
PAO1Δ*dipA* pP*cdrA*::*gfp*ASV		this study

PAO1Δ*wspR* attCTX::PwspA::*wspR* pMH489		this study
PAO1Δ*wspR* attCTX::PwspA::*wspR* pP*cdrA*::*gfp*ASV		this study
PAO1Δ*sadC* att::*sadC* pMH489		this study
PAO1Δ*sadC* att::*sadC* pP*cdrA*::*gfp*ASV		this study
PA14 Δ*wspF* pMH489		this study
PA14 Δ*wspF* pP*cdrA*::*gfp*ASV		this study
PA14 Δ*wspR* pMH489		this study
PA14 Δ*wspR* pP*cdrA*::*gfp*ASV		this study
PAO1Δ*wspR* attCTX::PBAD-wspR-eYFP pP*cdrA*::*mTFP1*		this study
PAO1Δ*wspR* attCTX::PBAD-wspR[L170D]-eYFP pP*cdrA*::*mTFP1*		this study
PAO1Δ*wspR* attCTX::PBAD-wspR[E253A]-eYFP pP*cdrA*::*mTFP1*		this study
PAO1 attCTX:: *bphS* attMiniTn7:: *mCherry* pP*cdrA*::*gfp*ASV		this study
PAO1 attMiniTn7:: *mCherry* pP*cdrA*::*gfp*ASV		this study
***E. coli* Strains**		
E. coli S17.1 pENTRPEX18Gm::Δ*pilY1*	conjugation proficient E. coli harboring *pilY1* deletion allele	Gift from Joe Harrison
E. coli S17.1 pENTRPEX18Gm::Δ*dipA*	conjugation proficient E. coli harboring *dipA* deletion allele	Gift from Joe Harrison
E. coli DH5α pUC18-miniTn7T2-P*cdrA*-RBSg10L-*gfp*AGA	source of P*cdrA*-RBSg10L	this study
E. coli DH5α pBBR1MCS5-PcdrA::RBSg10L::mTFP1	referred to as "pP*cdrA*::*mTFP1*"	this study
E. coli DH5α pP*siaA*::*gfp*	plasmid-based, fluorescent *siaA* transcriptional reporter	this study
Primers		
PAO1pilY1-SEQ-F	CTACTACGAGACCAATAGCGTC	this study
PAO1pilY1-SEQ-R	GTCGATGTCCACCAGGTTCTTC	this study
PAO1dipA-SEQ-F	GATACGCTTAACTTGGGCCCTG	this study
PAO1dipA-SEQ-R	CTTTTCTTGGTGAGGATTTCAGAAC	this study
PA14wspR-SEQ-F	GCTTCCTCACCATCGCCC	this study

PA14wspR-SEQ-R	CAGGTCGTCCAGGGTTTCC	this study
PA14wspF-SEQ-F	CTCACGGTGCGTGAGCTG	this study
PA14wspF-SEQ-R	GGTCCTGGAGGATCACCG	this study
SacI – PcdrA - F	GGGGAGCTC GTATGGAAGGTTCCTTGGCGG	this study
SOE-PcdrA-RBSg10L - R	ctcctcgcccttgctcaccat GGATATATCTCCTTCTTAAAG	this study
mTFP1 - F	atggtgagcaagggcgaggag	this study
KpnI - mTFP1 – R	GGGGTACC ttacttgtacagctcgtcc	this study
BamH1-Psia-F	GGG GGATCC GGCAGCGGCAACCGCCTCTG	this study
SiaA-BamH1-R	CCC GGATCC CAACCCCCAGTTCGCCGCCAT	this study
M13F(-21)	TGTAAAACGACGGCCAGT	GeneWiz
M13R	CAGGAAACAGCTATGAC	GeneWiz
ampR-F-qPCR	GCG CCA TCC CTT CAT CG	Colvin, 2011
ampR-R-qPCR	GAT GTC GAC GCG GTT GTT G	Colvin, 2011
pslA-F-qPCR	AAG ATC AAG AAA CGC GTG GAA T	Colvin, 2011
pslA-R-qPCR	TGT AGA GGT CGA ACC ACA CCG	Colvin, 2011
pelA-F-qPCR	CCT TCA GCC ATC CGT TCT TCT	Colvin, 2011
pelA-R-qPCR	TCG CGT ACG AAG TCG ACC TT	Colvin, 2011
rplU-F-qPCR	CGC AGT GAT TGT TAC CGG TG	Colvin, 2011
rplU-R-qPCR	AGG CCT GAA TGC CGG TGA TC	Colvin, 2011
OBT268	GGGGACAACTTTGTATACAAAGTTGTA CTATAGAGGGACAAACTCAAGGTCATTC GCAAGAGTGGCCTTTATGATTGACCTTC TTCCGGTTAATACGACCGGGATAACTCC ACTTGAGACGTGAAAAAAGAGGAGTAT TCATGCGTAAAGGAGAAGAACTTTTCAC TGGAG	This study
OBT269	GGGGACAAGTTTGTACAAAAAAGCAGG CTCGGCTTATTTGTATAGTTCATCCATGC CATGTGTAATC	This study
OBT314	CAGGTCGACTCTAGAGGATCCCCATCAG AAAATTTATCAAAAAGAGTGTTGACTTG TGAGCGGATAACAATGATACTTAGATTC AATTGTGAGCGGATAACAATTTCACACA TCTAGAATTAAAGAGGAGAAATTAAGC ATGGTGAGCAAGGGCGAGGAG	Zhao, 2013
OBT315	CTCCTCGCCCTTGCTCACCATGCTTAATT TCTCCTCTTTAATTCTAGATGTGTGAAAT TGTTATCCGCTCACAATTGAATCTAAGT ATCATTGTTATCCGCTCACAAGTCAACA CTCTTTTTGATAAATTTTCTGATGGGGAT CCTCTAGAGTCGACCTG	Zhao, 2013
pP*cdrA::gfp*ASV	PcdrA reporter with short halflife GFP	Rybtke, 2012

pENTRPEX18Gm::Δ*pilY1*	suicide plasmid containing *pilY1* deletion construct for use in PAO1	Gift from Joe Harrison
pENTRPEX18Gm::Δ*dipA*	suicide plasmid containing dipA deletion construct for use in PAO1	Gift from Joe Harrison
pBBR1MCS5	broad host range vector that is stable in *P. aeruginosa*, GentR	Kovach, 1995
pUC18-miniTn7T2-P*cdrA*-RBSg10L-*gfp*AGA	source plasmid containing promoter of *cdrA* with enhanced ribosomal binding site	this study
pNCS-mTFP1	source plasmid containing mTFP1	Allele Biotech
pBBR1MCS5-PcdrA::RBSg10L::mTFP1	teal fluorescent protein version of P*cdrA* reporter	this study
p*PsiaA::gfp*	P*siaA* reporter expressing stable GFP, constructed using pMH487 plasmid	this study
pBT270	miniTn7 transposon with *gfpmut3* driven by the A1/04/03 promoter; Ap^r, Gm^r	This study
pTNS2	T7 transposase expression vector	Choi, 2006
pBT223	miniTn7 transposon with *gfpmut3* driven by the *trc* promoter; Ap^r, Gm^r	This study
pBT212	A GateWay compatible plasmid containing *gfpmut3* flanked by attR5 and attL1 recombination sites; Km^r	This study
pBT200	A GateWay compatible plasmid containing the *trc* promoter flanked by attL2 and attL5 recombination sites; Kn^r	Zhao, 2013
pUC18-miniTn7T2-Gm-GW	A GateWay compatible mini-Tn7 based vector; Cm^r, Ap^r and Gm^r;	Zhao, 2013
AKN66	source for *gfpmut3*	Lambertsen, 2004)
pDONR221 P1-P5r	A GateWay compatible vector with attP1 and attP5r recombination sites and *ccdB*; Kn^r and Cm^r	Invitrogen

878 **References**

879 1. M. E. Davey, G. A. O'toole, Microbial biofilms: from ecology to molecular genetics.
880 *Microbiol. Mol. Biol. Rev. MMBR*. **64**, 847–867 (2000).

881 2. U. Römling, M. Y. Galperin, M. Gomelsky, Cyclic di-GMP: the First 25 Years of a
882 Universal Bacterial Second Messenger. *Microbiol. Mol. Biol. Rev. MMBR*. **77**, 1–52
883 (2013).

884 3. L. Ma *et al.*, Assembly and development of the Pseudomonas aeruginosa biofilm
885 matrix. *PLoS Pathog.* **5**, e1000354 (2009).

886 4. K. M. Colvin *et al.*, The Pel Polysaccharide Can Serve a Structural and Protective
887 Role in the Biofilm Matrix of Pseudomonas aeruginosa. *PLoS Pathog*. **7**, e1001264
888 (2011).

889 5. Y. Irie *et al.*, Self-produced exopolysaccharide is a signal that stimulates biofilm
890 formation in Pseudomonas aeruginosa. *Proc. Natl. Acad. Sci.* **109**, 20632–20636
891 (2012).

892 6. N. Billings *et al.*, The Extracellular Matrix Component Psl Provides Fast-Acting
893 Antibiotic Defense in Pseudomonas aeruginosa Biofilms. *PLoS Pathog*. **9**,
894 e1003526 (2013).

895 7. K. Zhao *et al.*, Psl trails guide exploration and microcolony formation in
896 Pseudomonas aeruginosa biofilms. *Nature*. **497**, 388–391 (2013).

897 8. C. R. Armbruster *et al.*, Staphylococcus aureus Protein A Mediates Interspecies
898 Interactions at the Cell Surface of Pseudomonas aeruginosa. *mBio*. **7** (2016),
899 doi:10.1128/mBio.00538-16.

900 9. Q. Wei, L. Z. Ma, Biofilm Matrix and Its Regulation in Pseudomonas aeruginosa. *Int.*
901 *J. Mol. Sci.* **14**, 20983–21005 (2013).

902 10. M. Starkey *et al.*, Pseudomonas aeruginosa rugose small-colony variants have
903 adaptations that likely promote persistence in the cystic fibrosis lung. *J. Bacteriol.*
904 **191**, 3492–3503 (2009).

905 11. A. I. Chen *et al.*, Candida albicans Ethanol Stimulates Pseudomonas aeruginosa
906 WspR-Controlled Biofilm Formation as Part of a Cyclic Relationship Involving
907 Phenazines. *PLOS Pathog.* **10**, e1004480 (2014).

908 12. V. Huangyutitham, Z. T. Güvener, C. S. Harwood, Subcellular Clustering of the
909 Phosphorylated WspR Response Regulator Protein Stimulates Its Diguanylate
910 Cyclase Activity. *mBio*. **4** (2013), doi:10.1128/mBio.00242-13.

911 13. Y. Luo *et al.*, A Hierarchical Cascade of Second Messengers Regulates Pseudomonas
912 aeruginosa Surface Behaviors. *mBio*. **6** (2015), doi:10.1128/mBio.02456-14.

14. S. L. Kuchma *et al.*, Cyclic-di-GMP-Mediated Repression of Swarming Motility by Pseudomonas aeruginosa: the pilY1 Gene and Its Impact on Surface-Associated Behaviors. *J. Bacteriol.* **192**, 2950–2964 (2010).

15. A. Persat, Y. F. Inclan, J. N. Engel, H. A. Stone, Z. Gitai, Type IV pili mechanochemically regulate virulence factors in Pseudomonas aeruginosa. *Proc. Natl. Acad. Sci.* **112**, 7563–7568 (2015).

16. J. R. O'Connor, N. J. Kuwada, V. Huangyutitham, P. A. Wiggins, C. S. Harwood, Surface sensing and lateral subcellular localization of WspA, the receptor in a chemosensory-like system leading to c-di-GMP production. *Mol. Microbiol.* **86**, 720–729 (2012).

17. J. W. Hickman, C. S. Harwood, Identification of FleQ from Pseudomonas aeruginosa as a c-di-GMP-responsive transcription factor. *Mol. Microbiol.* **69**, 376–389 (2008).

18. C. Baraquet, K. Murakami, M. R. Parsek, C. S. Harwood, The FleQ protein from Pseudomonas aeruginosa functions as both a repressor and an activator to control gene expression from the pel operon promoter in response to c-di-GMP. *Nucleic Acids Res.* **40**, 7207–7218 (2012).

19. M. T. Rybtke *et al.*, Fluorescence-Based Reporter for Gauging Cyclic Di-GMP Levels in Pseudomonas aeruginosa. *Appl. Environ. Microbiol.* **78**, 5060–5069 (2012).

20. C. Baraquet, C. S. Harwood, FleQ DNA Binding Consensus Sequence Revealed by Studies of FleQ-Dependent Regulation of Biofilm Gene Expression in Pseudomonas aeruginosa. *J. Bacteriol.* **198**, 178–186 (2015).

21. L. K. Jennings *et al.*, Pel is a cationic exopolysaccharide that cross-links extracellular DNA in the Pseudomonas aeruginosa biofilm matrix. *Proc. Natl. Acad. Sci. U. S. A.* **112**, 11353–11358 (2015).

22. H. Kulesekara *et al.*, Analysis of Pseudomonas aeruginosa diguanylate cyclases and phosphodiesterases reveals a role for bis-(3′-5′)-cyclic-GMP in virulence. *Proc. Natl. Acad. Sci. U. S. A.* **103**, 2839–2844 (2006).

23. C. K. Lee *et al.*, Multigenerational memory and adaptive adhesion in early bacterial biofilm communities. *Proc. Natl. Acad. Sci.* **115**, 4471 (2018).

24. J. Ribbe, A. E. Baker, S. Euler, G. A. O'Toole, B. Maier, Role of Cyclic Di-GMP and Exopolysaccharide in Type IV Pilus Dynamics. *J. Bacteriol.* **199**, e00859-16 (2017).

25. M.-H. Ryu, M. Gomelsky, Near-infrared Light Responsive Synthetic c-di-GMP Module for Optogenetic Applications. *ACS Synth. Biol.* **3**, 802–810 (2014).

948 26. M. Ackermann, A functional perspective on phenotypic heterogeneity in
949 microorganisms. *Nat Rev Micro*. **13**, 497–508 (2015).

950 27. D. Dubnau, R. Losick, Bistability in bacteria. *Mol. Microbiol.* **61**, 564–572 (2006).

951 28. M. B. Elowitz, A. J. Levine, E. D. Siggia, P. S. Swain, Stochastic Gene Expression in
952 a Single Cell. *Science*. **297**, 1183 (2002).

953 29. J. Casadesús, D. Low, Epigenetic Gene Regulation in the Bacterial World. *Microbiol.*
954 *Mol. Biol. Rev.* **70**, 830–856 (2006).

955 30. B.-J. Laventie *et al.*, A Surface-Induced Asymmetric Program Promotes Tissue
956 Colonization by Pseudomonas aeruginosa. *Cell Host Microbe*. **25**, 140-152.e6
957 (2019).

958 31. B. R. Kulasekara *et al.*, c-di-GMP heterogeneity is generated by the chemotaxis
959 machinery to regulate flagellar motility. *eLife*. **2**, e01402 (2013).

960 32. H. J. VOGEL, D. M. BONNER, Acetylornithinase of Escherichia coli: partial
961 purification and some properties. *J. Biol. Chem.* **218**, 97–106 (1956).

962 33. L. R. Hmelo *et al.*, Precision-engineering the Pseudomonas aeruginosa genome with
963 two-step allelic exchange. *Nat Protoc.* **10**, 1820–1841 (2015).

964 34. K.-H. Choi, H. P. Schweizer, mini-Tn7 insertion in bacteria with single attTn7 sites:
965 example Pseudomonas aeruginosa. *Nat. Protoc.* **1**, 153 (2006).

966 35. M. Lanzer, H. Bujard, Promoters largely determine the efficiency of repressor action.
967 *Proc. Natl. Acad. Sci. U. S. A.* **85**, 8973–8977 (1988).

968 36. T. T. Hoang, A. J. Kutchma, A. Becher, H. P. Schweizer, Integration-Proficient
969 Plasmids for Pseudomonas aeruginosa: Site-Specific Integration and Use for
970 Engineering of Reporter and Expression Strains. *Plasmid*. **43**, 59–72 (2000).

971 37. K. M. Colvin *et al.*, The Pel and Psl polysaccharides provide Pseudomonas
972 aeruginosa structural redundancy within the biofilm matrix. *Environ. Microbiol.* **14**,
973 1913–1928 (2012).

974 38. B. R. Borlee *et al.*, Pseudomonas aeruginosa uses a cyclic-di-GMP-regulated adhesin
975 to reinforce the biofilm extracellular matrix. *Mol. Microbiol.* **75**, 827–842 (2010).

976

977

Figure 1 – Supplement 1

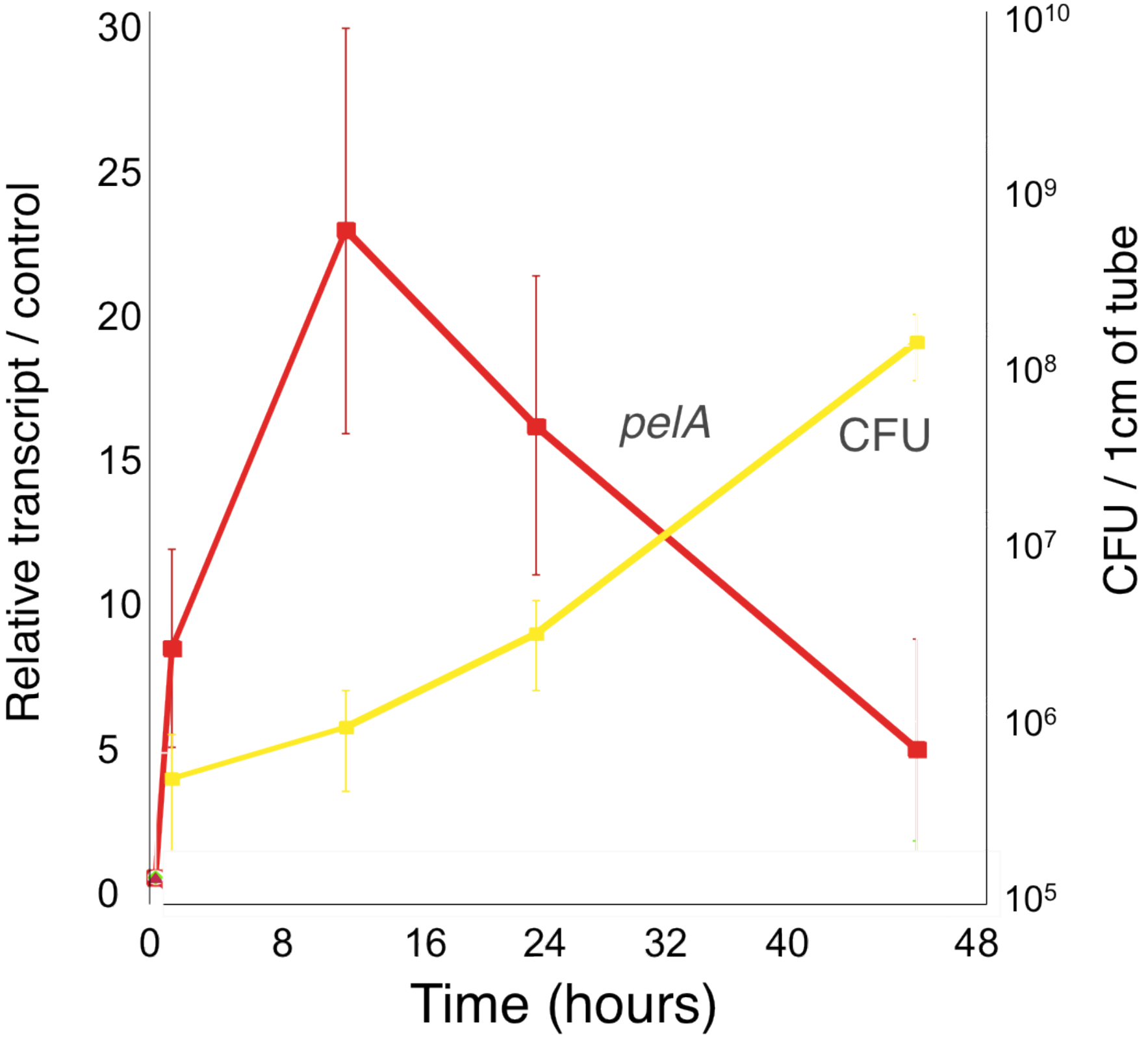

Figure 1—Supplement 2

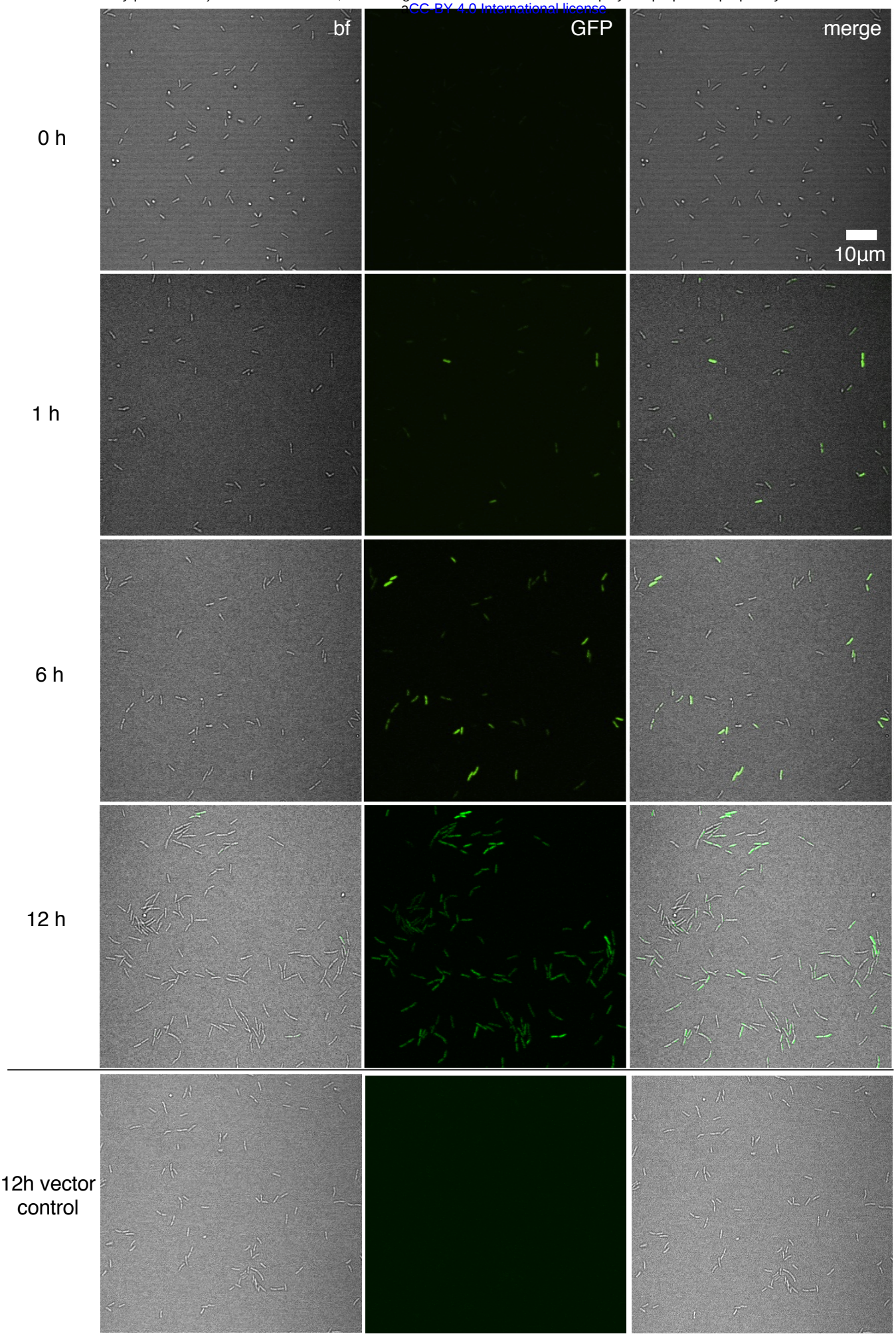

Figure 1 – Supplement 3

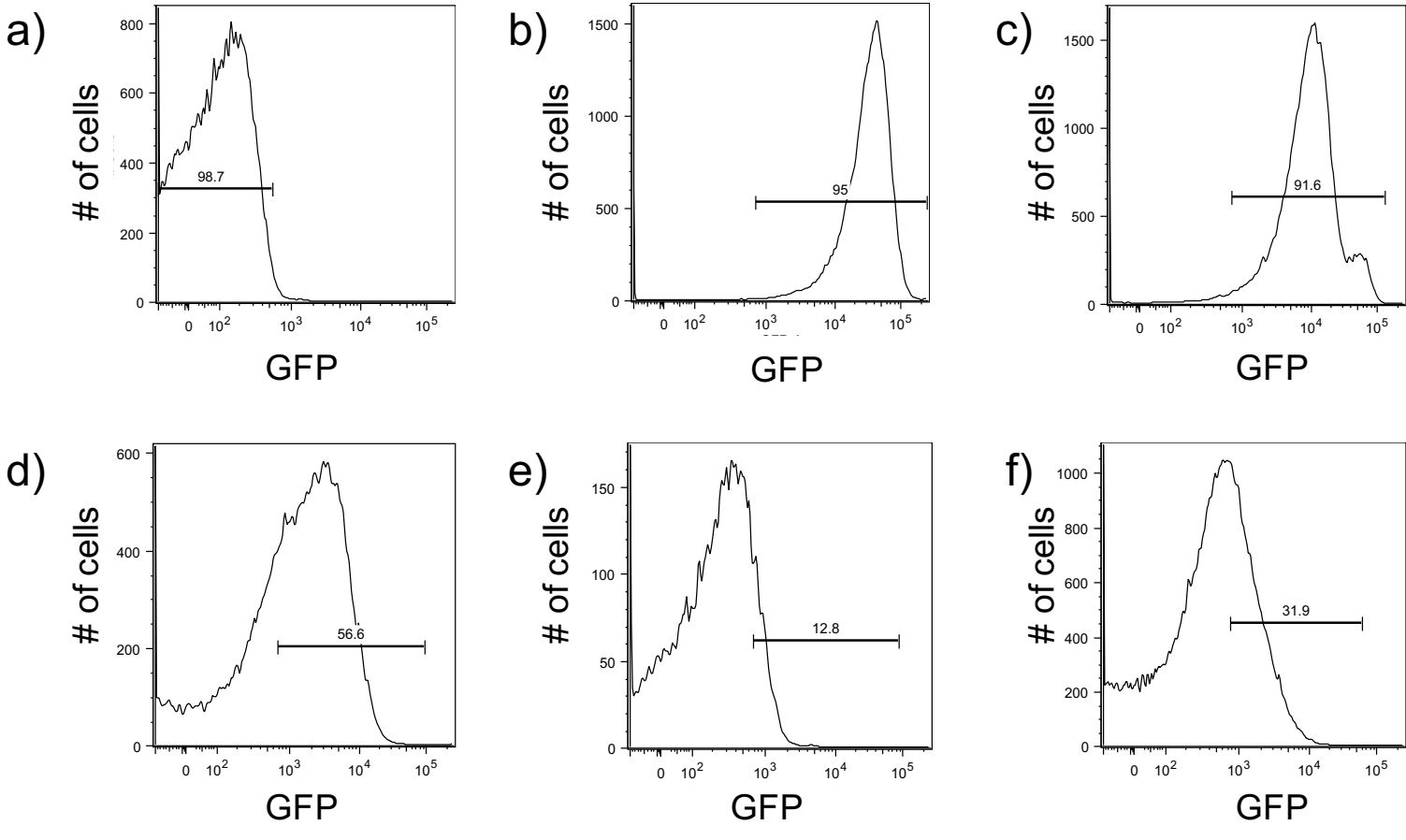

Figure 1 – Supplement 4

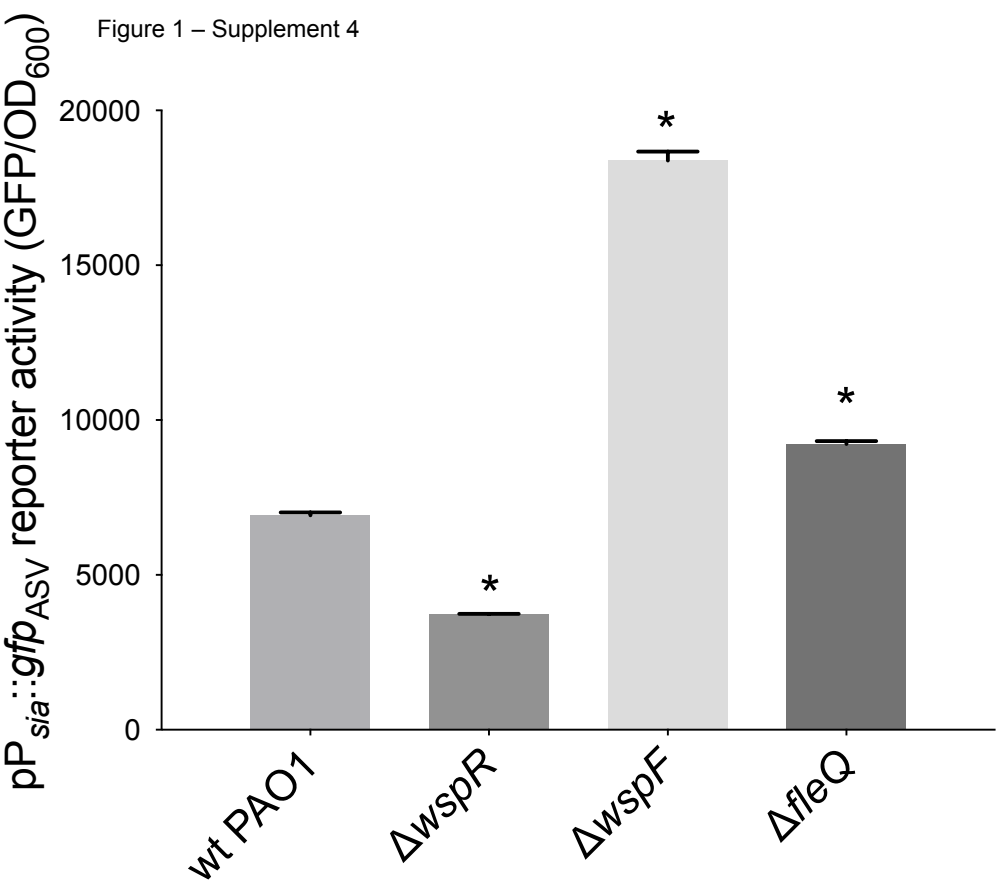

Figure 1 – Supplement 5

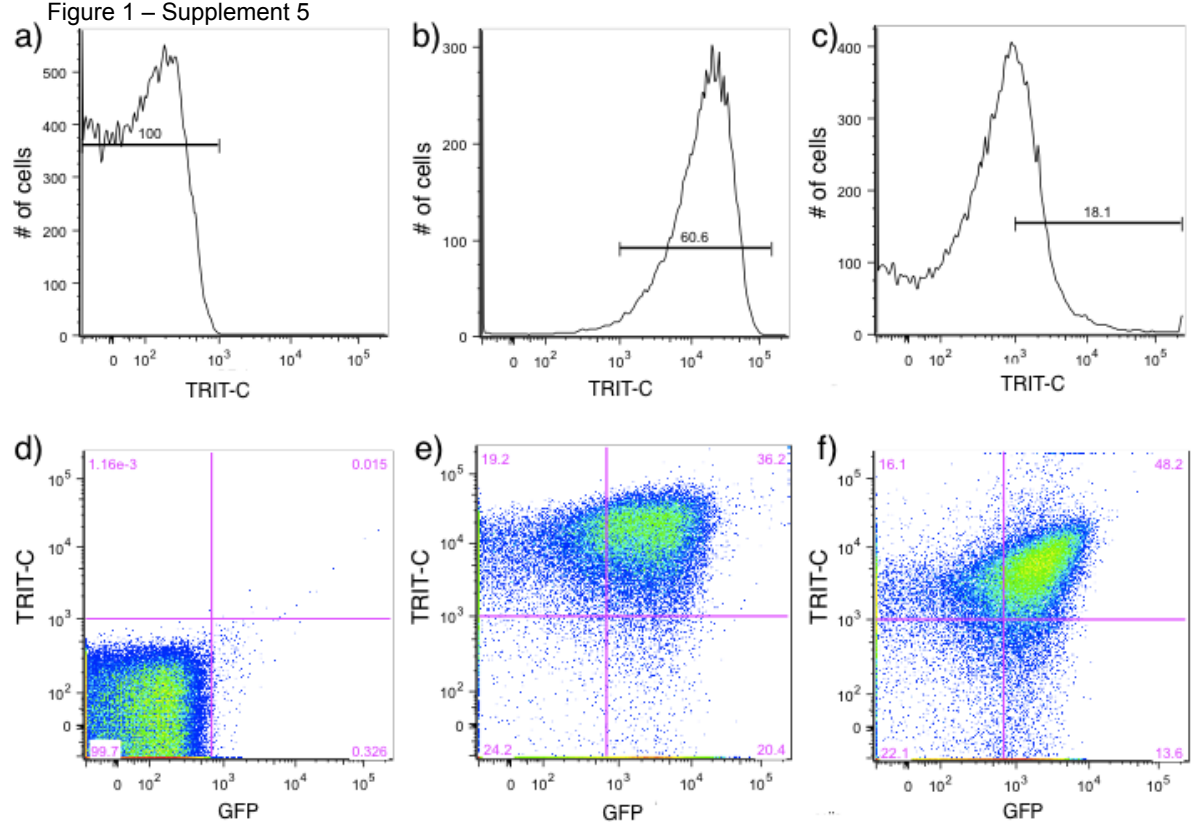

Figure 1 – Supplement 6

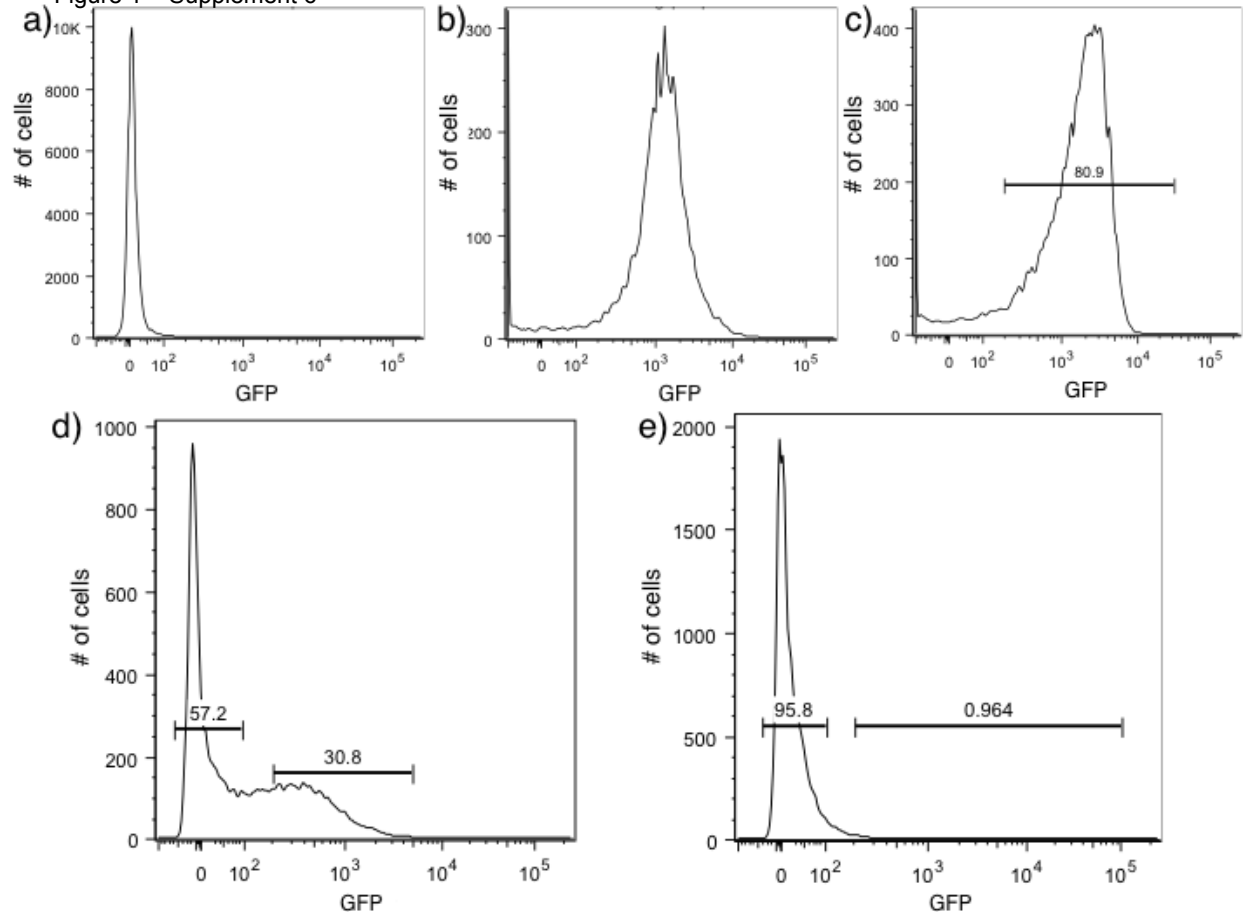

Figure 2 – Supplement 1

a)

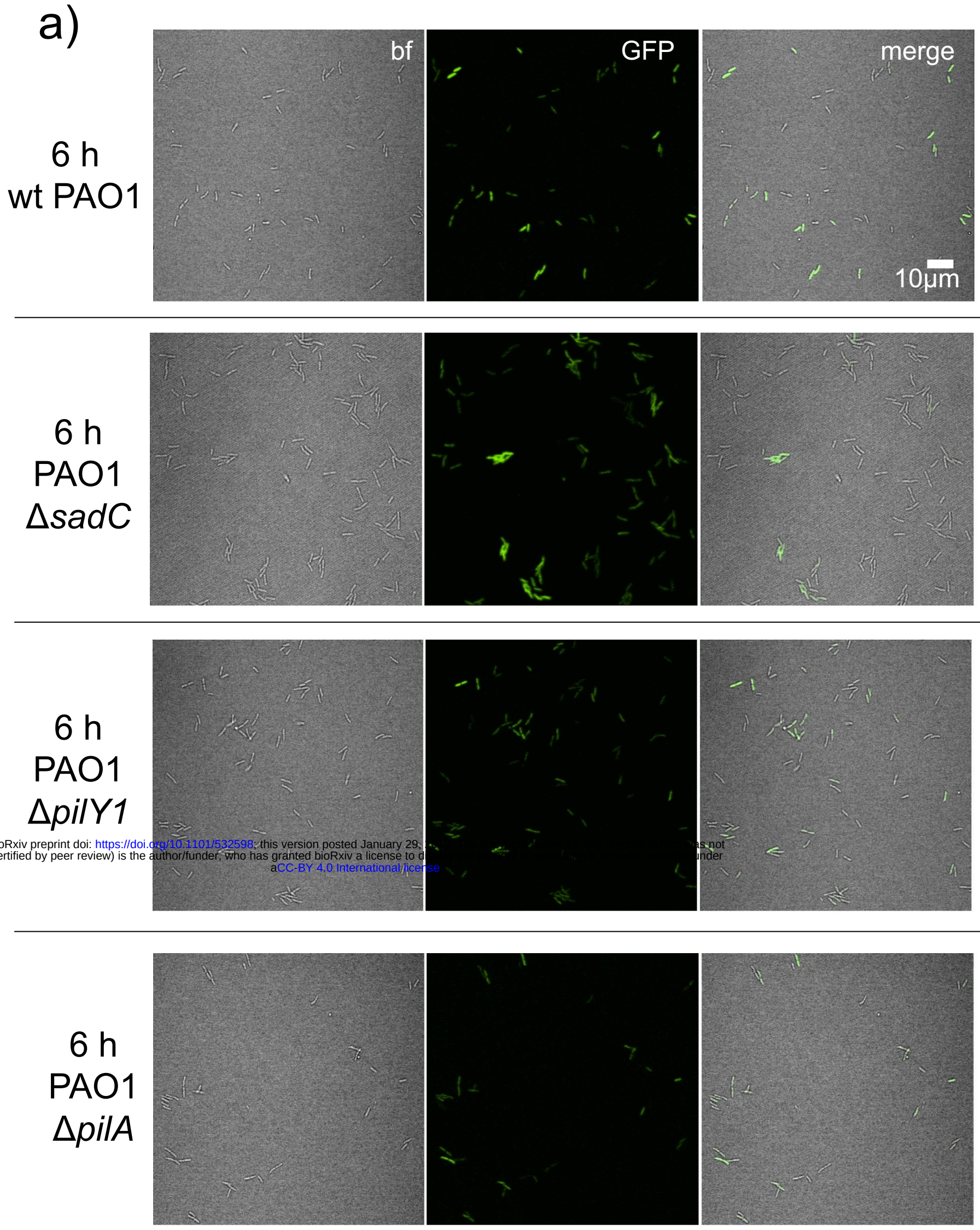

b)

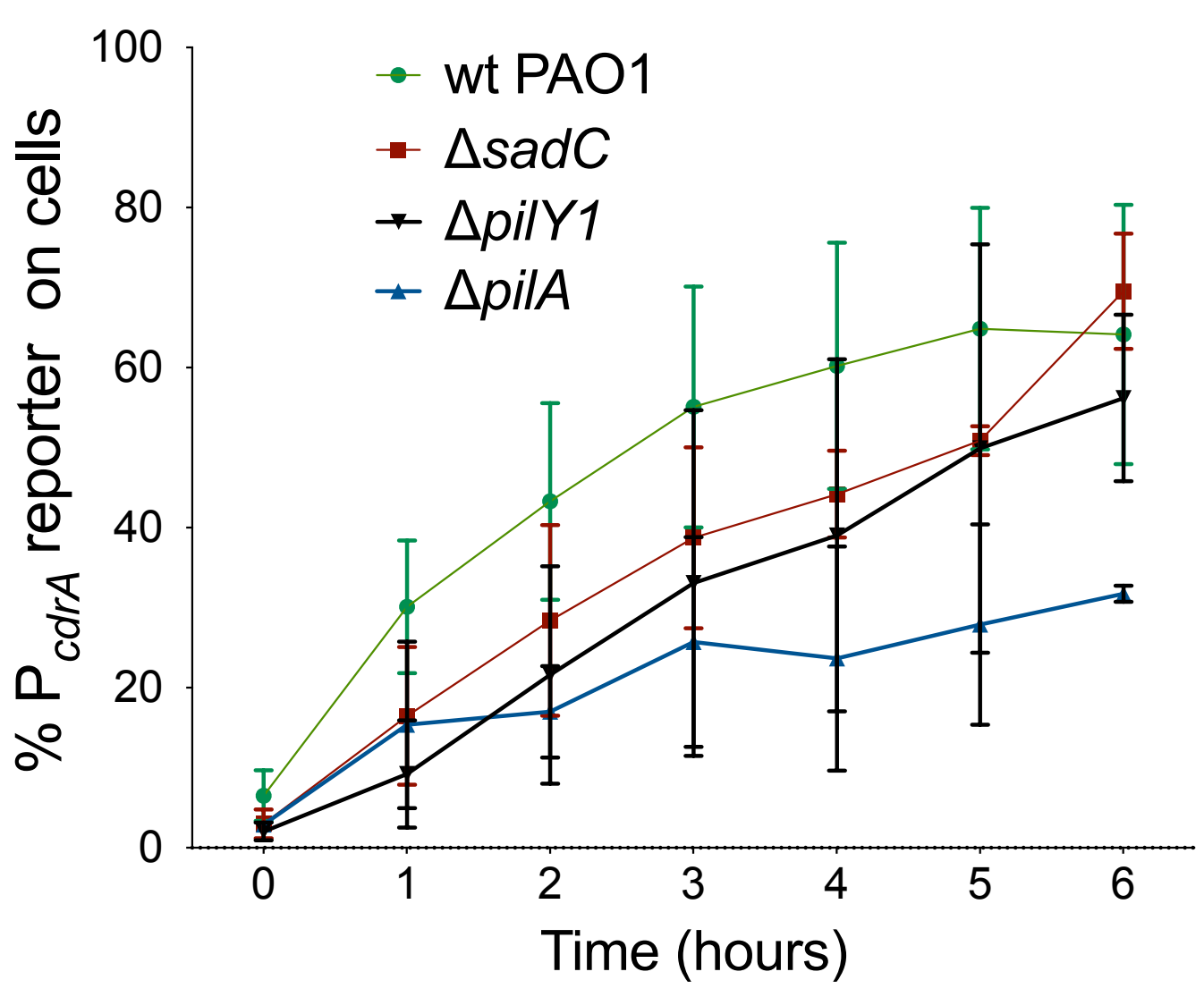

Figure 2 – Supplement 2

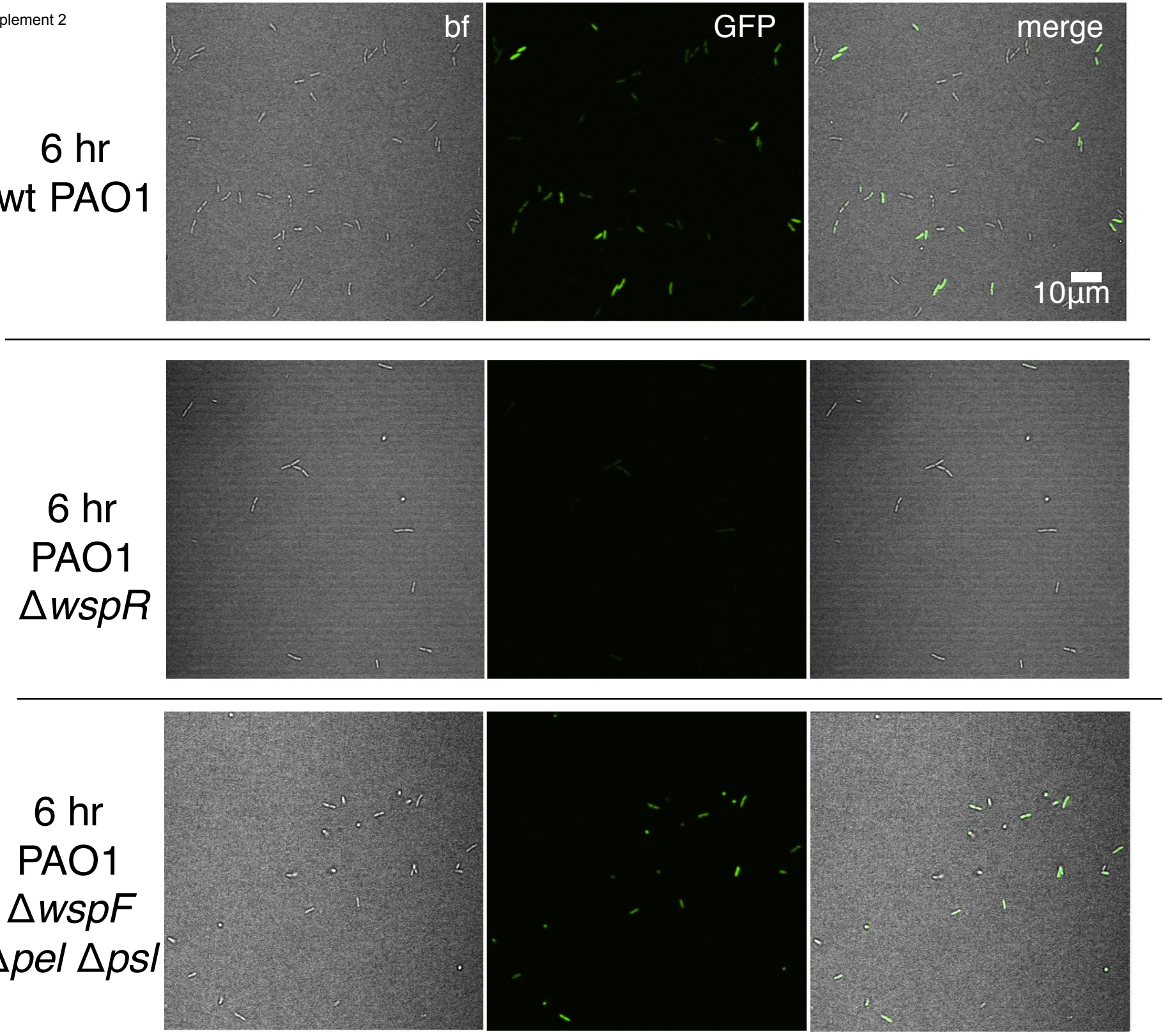

Figure 2 – Supplement 3

a)

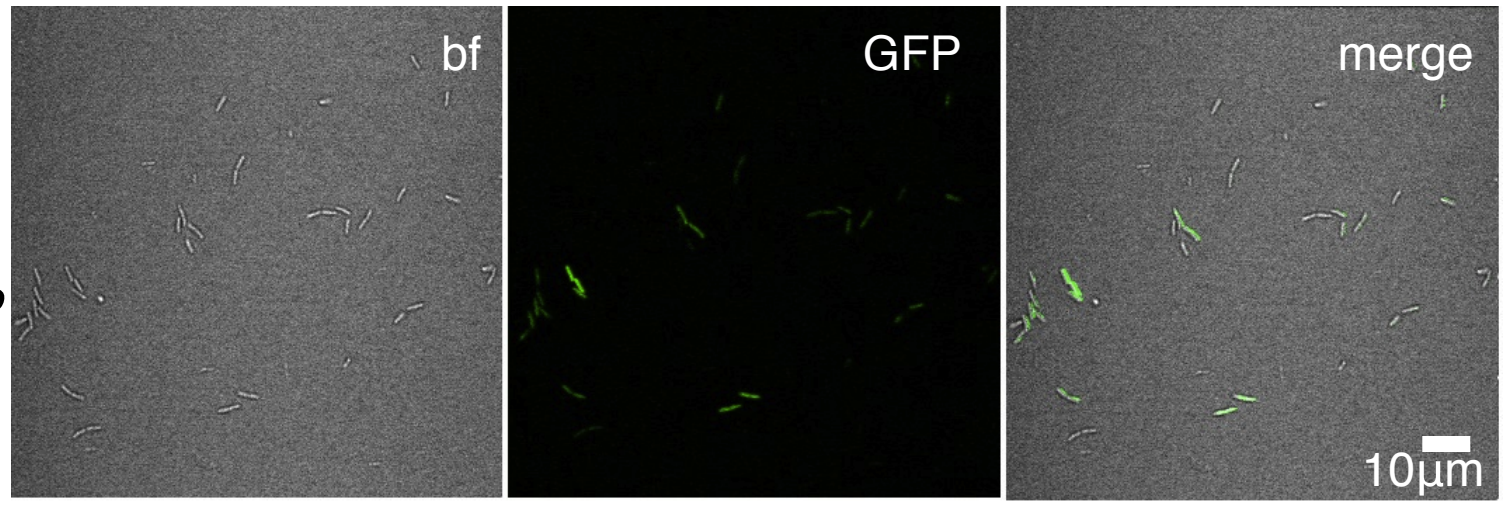

6 hr
PAO1
Δ*wspR::wspR*

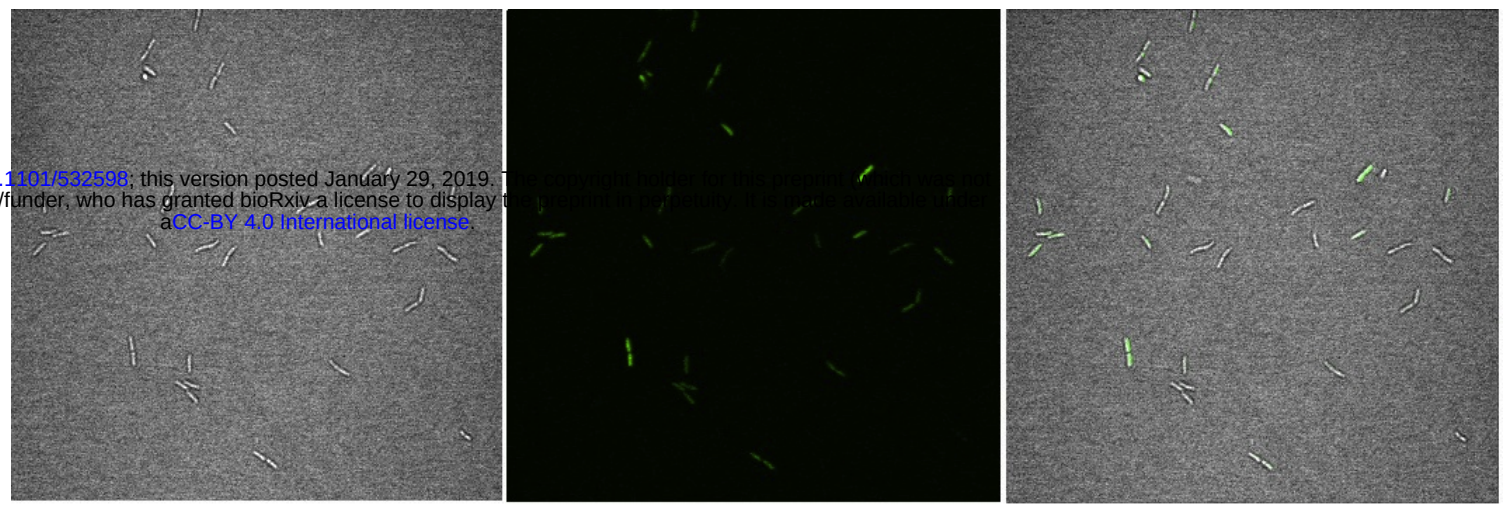

6hr
PAO1
Δ*sadC::sadC*

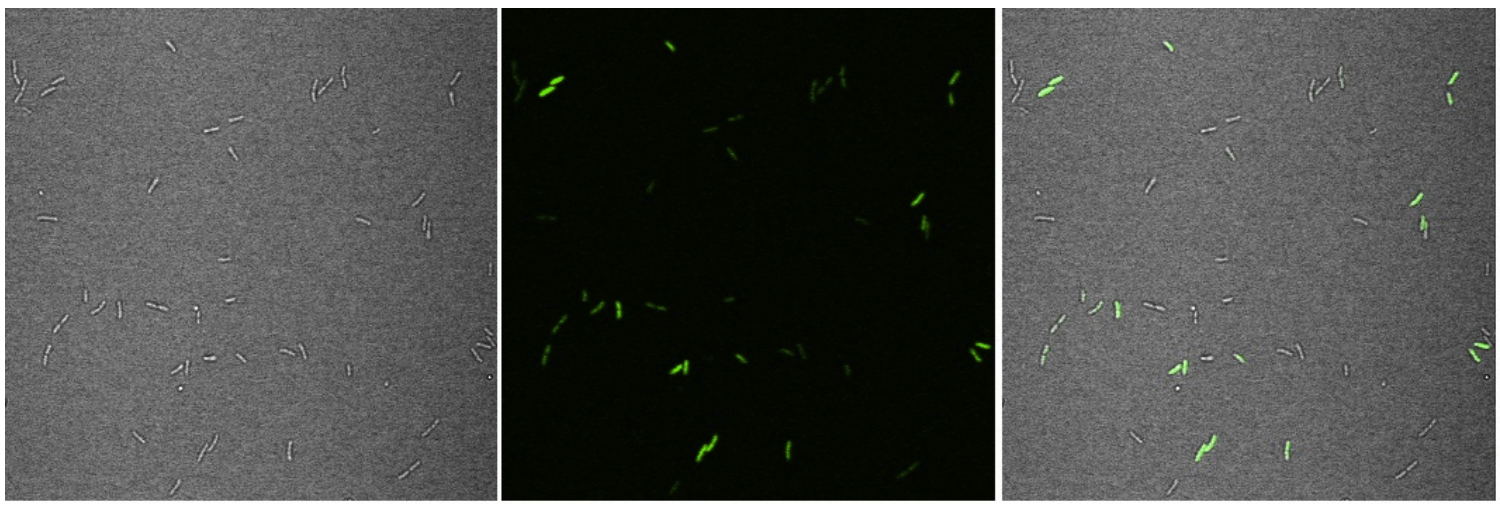

6hr

wt PAO1

b)

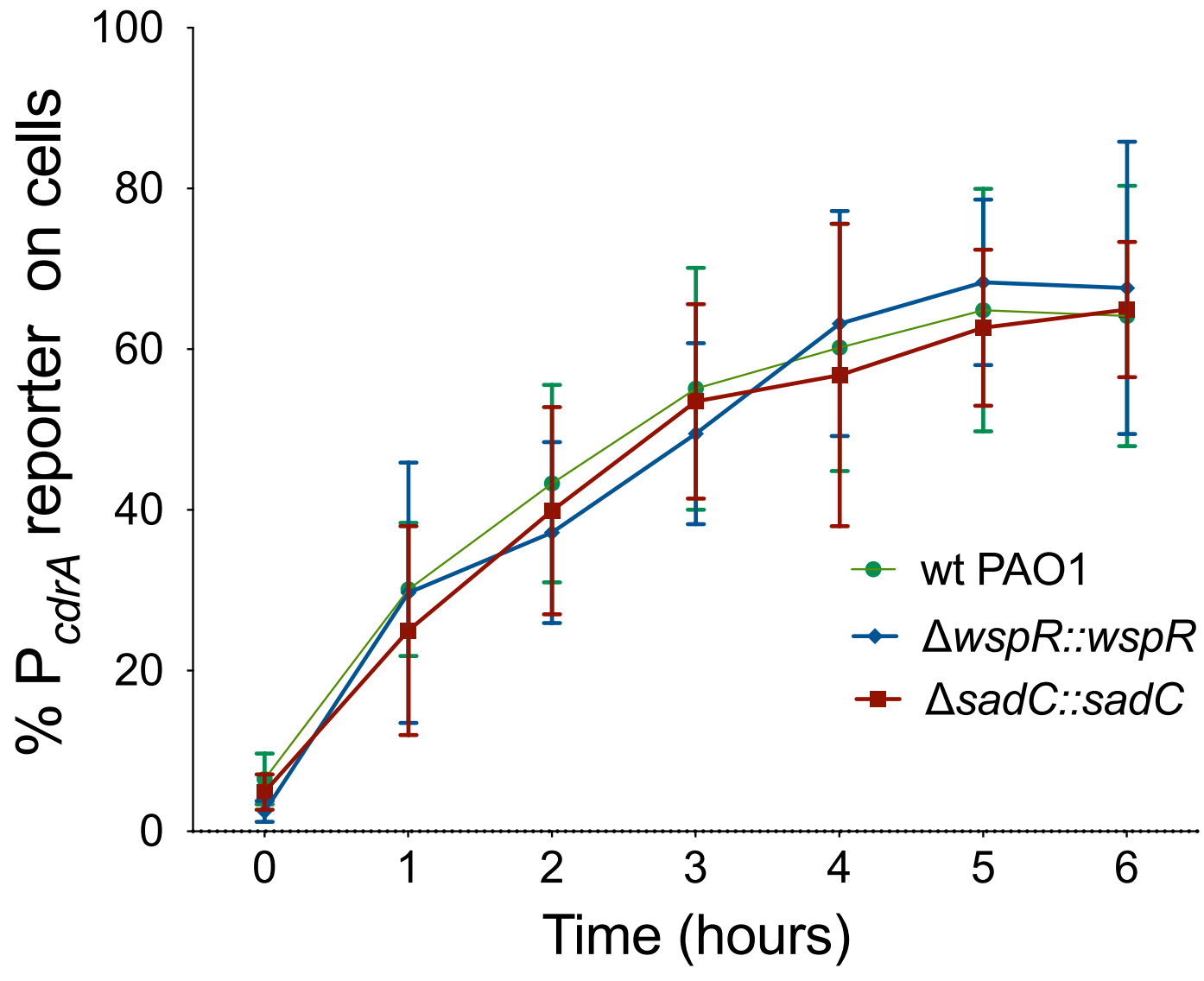

Figure 2 – Supplement 4

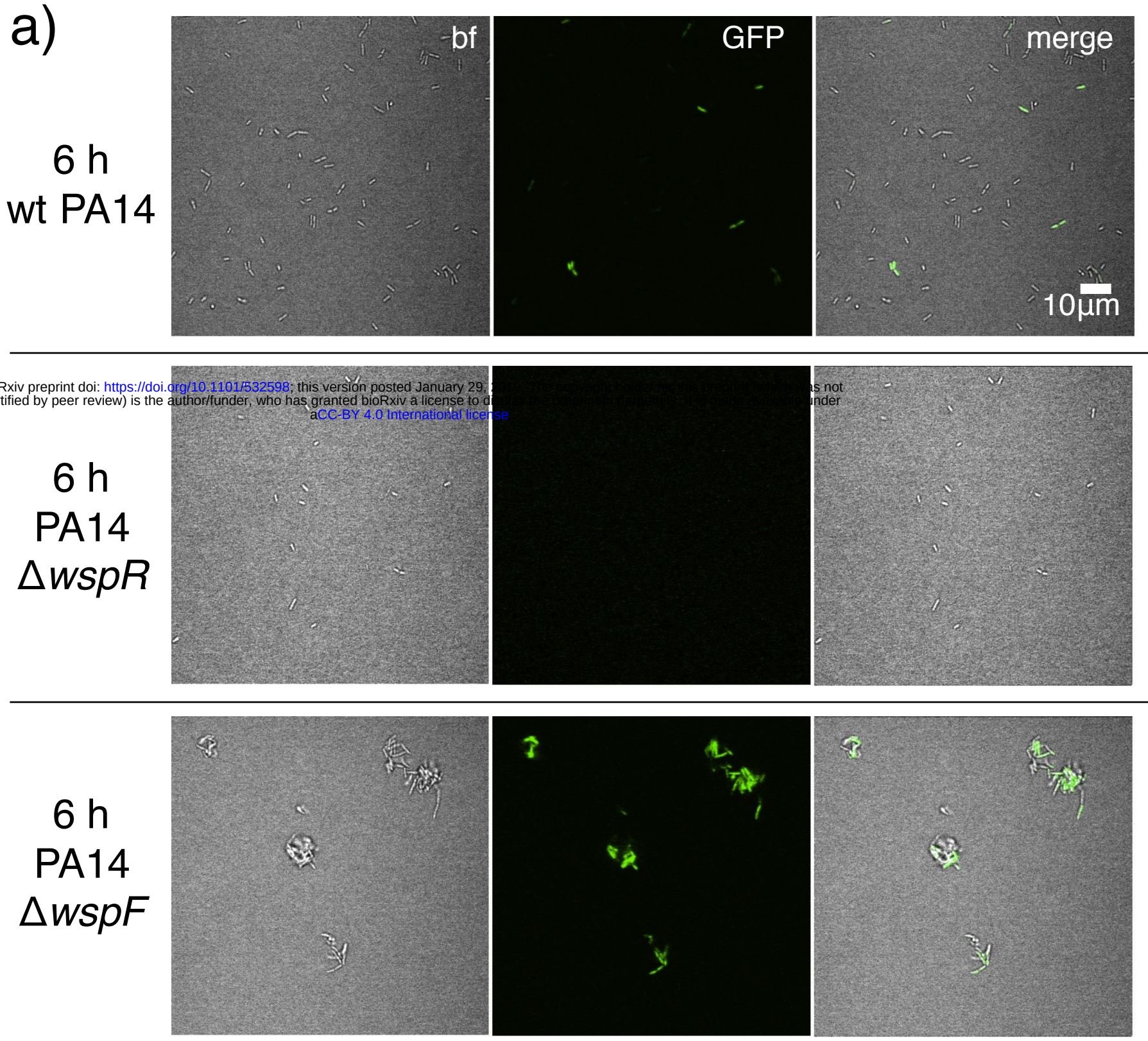

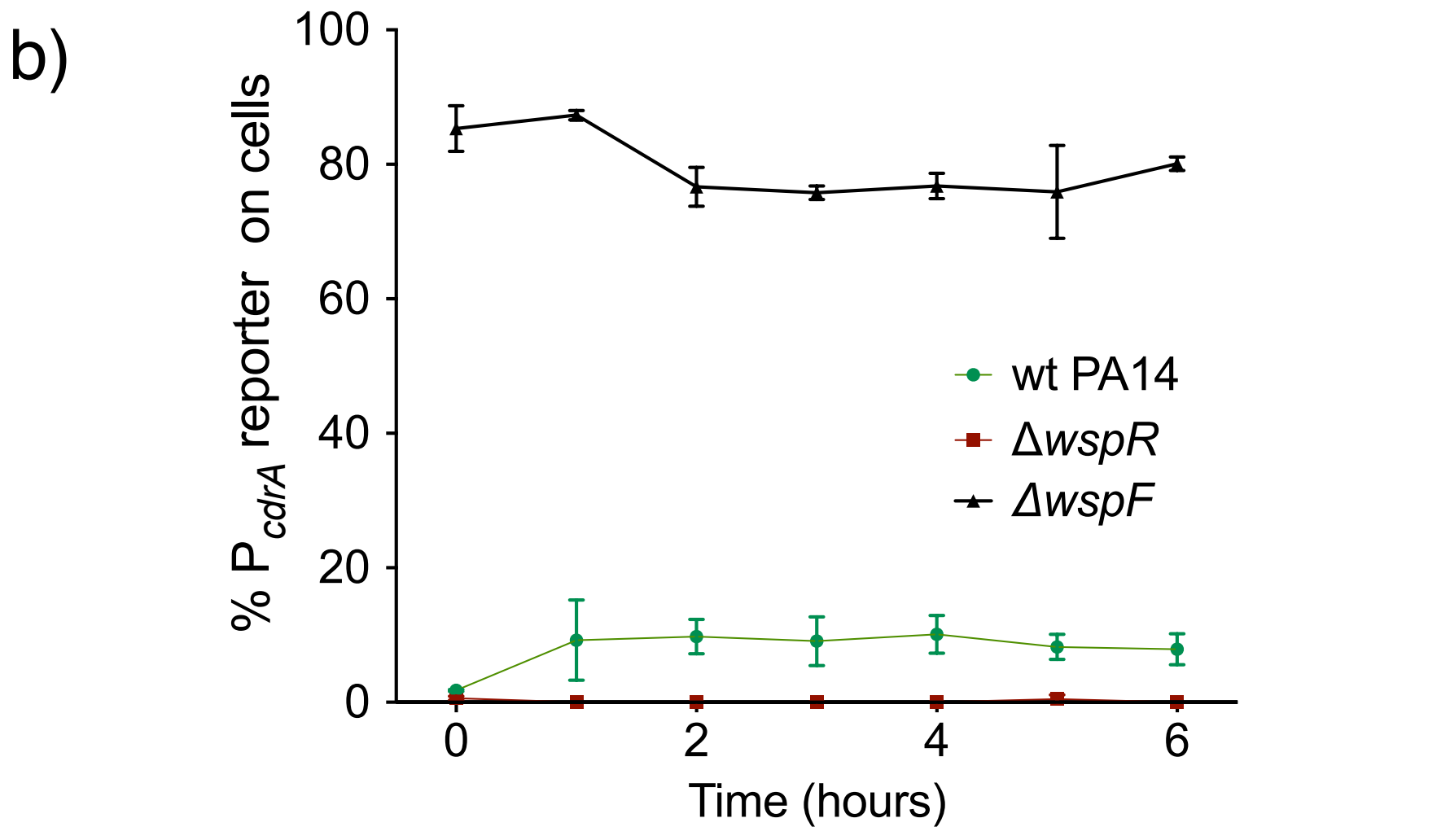

Figure 5 – Supplement 1

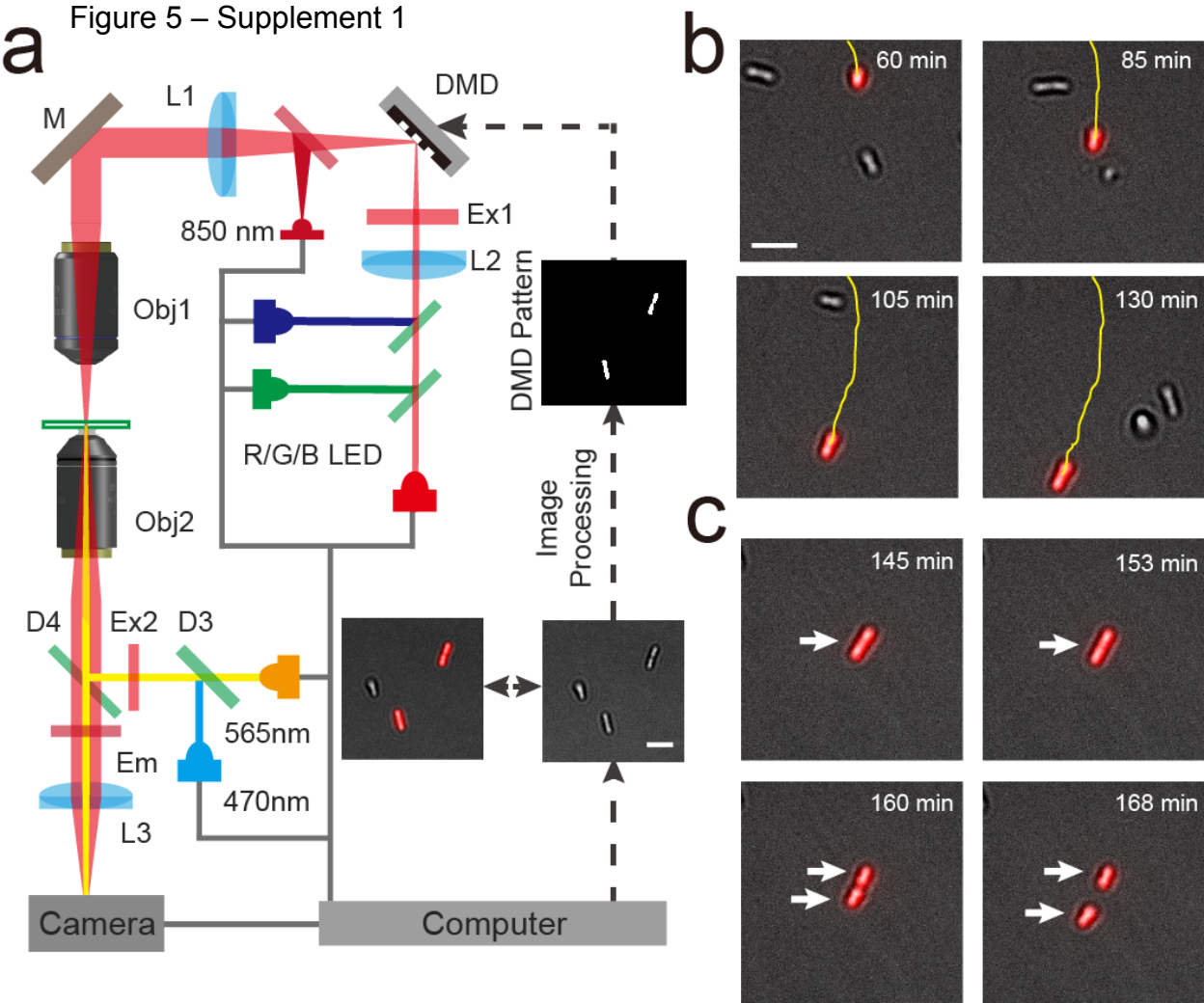

Figure 5 – Supplement 2